Development of a Magnetic Particle Tracking Technique using a Hybrid Numerical Optimization Algorithm

By

Rohan Kokate

Submitted to the Graduate degree program in Aerospace Engineering and the Graduate Faculty of the University of Kansas in partial fulfilment of the requirements for the degree of Master of Science in Aerospace Engineering.

_____

Chair: Dr. Huixuan Wu

_____

Dr. Saeed Farokhi

_____

Dr. Ray Taghavi

Date Defended: 16th June 2020

The thesis committee for Rohan Kokate certifies that this is the approved

version of the following thesis:

Development of a Magnetic Particle Tracking technique using a hybrid numerical optimization algorithm

_____

Chair: Dr. Huixuan Wu

_____

Dr. Saeed Farokhi

_____

Dr. Ray Taghavi

Date Approved: 16th June 2020

Abstract

This thesis focuses on the development of a 3D Magnetic Particle Tracking (MPT) technique using a hybrid numerical optimization algorithm which is able to reconstruct not only the particle's location but also its orientation in the given measurement domain. The MPT is an inexpensive particle tracking technique which can be used in both transparent and opaque working conditions and requires no specific safety precautions for its use. In this work, initially, the algorithm is tested for accuracy numerically for simulation cases with continuous velocity/acceleration, sudden acceleration, sudden rotation and the Brownian motion simulation. The accuracy of the algorithm is found to be comparable with the state-of-the-art optimization approach, but the reconstruction is orders of magnitude faster. The numerical simulation for the Brownian motion showed that the MPT position uncertainty can reach 0.86 % and the angular error is 1.5^{o} for a measurement domain with a size of about 10 cm. On validation from the above simulations, the MPT is tested in an experimental setup to study the dense granular shear flow. The MPT algorithm is used to track a cylindrical tracer particle of aspect ratio 1 encapsulated with a neodymium magnetic bead in a cylinder filled with plastic balls, which acts as the bulk material, of similar density. It is observed that the balls show a layered structure in both the X-Y position distribution and in the vertical direction. Because of the above advantages and its high accuracy, MPT is a powerful tool for studying dense granular flows and provide insight into this physical phenomenon.

Acknowledgements

I would like to first thank my parents, Uday Kokate and Aditi Kokate, for their undying love and support throughout my life. Without them, I would not be the person I am today. They are the pillars of my achievements. I would also like to give special thanks to Adriana Martinez, it was through her constant support, love and encouragement that I have been able to make it through this challenging period.

I owe all my research accomplishments to my advisor, Dr. Huixuan Wu who has always motivated me to work harder and produce better results. I could not have asked for a better advisor. My experience working in the Experimental Fluid and Applied Optics Lab has not only made me a better engineer, but also a better person. Thank you for everything, Dr. Wu.

I would like to thank Dr. Farokhi for his technical and moral support. Dr. Farokhi was kind enough to meet with me and answer any of my questions and queries with patience. His knowledge and experience in the field fluid dynamics was a major guiding factor for my progress. I would also like to thank Dr. Taghavi for his invaluable guidance.

Next, I would like to thank Xingtian Tao and the other graduate students at KU, without whom, I could not have made quick progress in my thesis. Finally, many thanks go to all my friends and colleagues. Thank you for understanding me and supporting me in all my endeavours.

Rohan Kokate

Table of Contents

List of figures

List of Tables

Nomenclature

Latin Letters

B	Magnetic flux density	T (N.m/A)
D	measurement or estimated sensor reading	~
N	total number of sensors	~
H	Magnetic field strength	A/m
m	Magnetic moment	$A.m^2$
L	Length between two sensors	m
r	the location of the magnet	m
r_o	the location of sensor	M
n	unit vector in the $r - r_0$ direction	

Greek Letters

Θ	angle between *n* and the *x*-axis	degree
β	angle between the sensor and the magnet in the Z plane	degree
ε	Gaussian random variable	~
μ	Magnetic permeability	N/A^2
μ_r	Relative permeability	~
μ_o	Absolute permeability	~

Abbreviations and Acronyms

AE	Acoustic Emissions
CGS	Centimetre-gram-second
HNM	Hybrid Numerical Method
MKS	Metre-Kilogram-second

MPT	Magnetic Particle tracking
RPT	Radioactive Particle tracking
PEPT	Positron emission particle tracking
PET	Positron Emission Tomography
PIV	Particle Image Velocimetry
MMM	Magnetic Marker Monitoring
GM	Gradient Method
SIR	Sequential Importance sampling with Resampling
SQP	Sequential Quadratic Programming
EKF	Extended Kalman Filter
LM	Levenberg–Marquardt
LoR	Line of Response
2D	Two dimensional
3D	Three dimensional

1. Introduction

1.1 Thesis Roadmap

It is not possible in every situation to have a window of observation to analyse and understand the complex nature of fluid particle dynamics. Therefore, it is necessary to have a technique which can give us details about such complex flow dynamics without having a direct image of the flow environment. This thesis focuses on the development of a 3D Magnetic Particle Tracking (MPT) algorithm which is able to reconstruct not only the particle location but also its orientation in the given flow domain. Most of the techniques available in literature concentrate only on the position of the particle in the system but in a 3D environment, the orientation of the particle is an equally important parameter to be considered. MPT is an inexpensive particle tracking technique which can be used in both transparent and opaque working conditions and requires no specific safety conditions for its use. We use a hybrid numerical gradient based optimization method to reconstruct the position of the particle in the given domain based on the MPT principle. The 2D analytical and 3D numerical solutions are presented in chapter 2 and 3. Different optimization techniques available in literature are also described in chapter 3. In this work, initially, the MPT reconstruction algorithm is tested for accuracy using numerical simulation for cases with continuous velocity/acceleration, sudden acceleration, sudden rotation and eventually the Brownian motion simulation. Since Brownian motion is as random as a particle motion can get, if the algorithm can reconstruct such a motion, it should be able to track any kind of motion in three dimensions. The algorithm's performance is tested and compared with other popular optimization techniques available in literature. On validation from the above simulations, the proposed MPT algorithm is tested in an experimental setup to study the granular shear flow. The MPT algorithm is used to track a plastic cylindrical particle with

aspect ratio 1 encapsulated with a neodymium magnetic bead in a container filled with plastic balls of similar density. Because of the above advantages and its high accuracy, MPT is a powerful tool for studying dense granular flows and provide insight into this physical phenomenon.

1.2 Background

1.2.1 History of Particle Tracking

Roughly, 80% of information entering the human brain is through vision, and the brain is very powerful at processing images. Therefore, the idea of using qualitative observations and visualizations is a powerful tool. This can be used very effectively in the complex study of fluid dynamics. Flow visualization is a qualitative way to study any flow phenomenon. Even though it provides no specific number, it may lead to deep understanding of the physical problem at hand. While the method of adding particles or objects to a fluid is likely to have been used from time to time through the ages, no sustained application of the method is known. It was Ludwig Prandtl, in the early 20^{th} century, who came up with a systematic way to apply this method to study the dynamics of particles in a fluid flow (*Figure 1*).

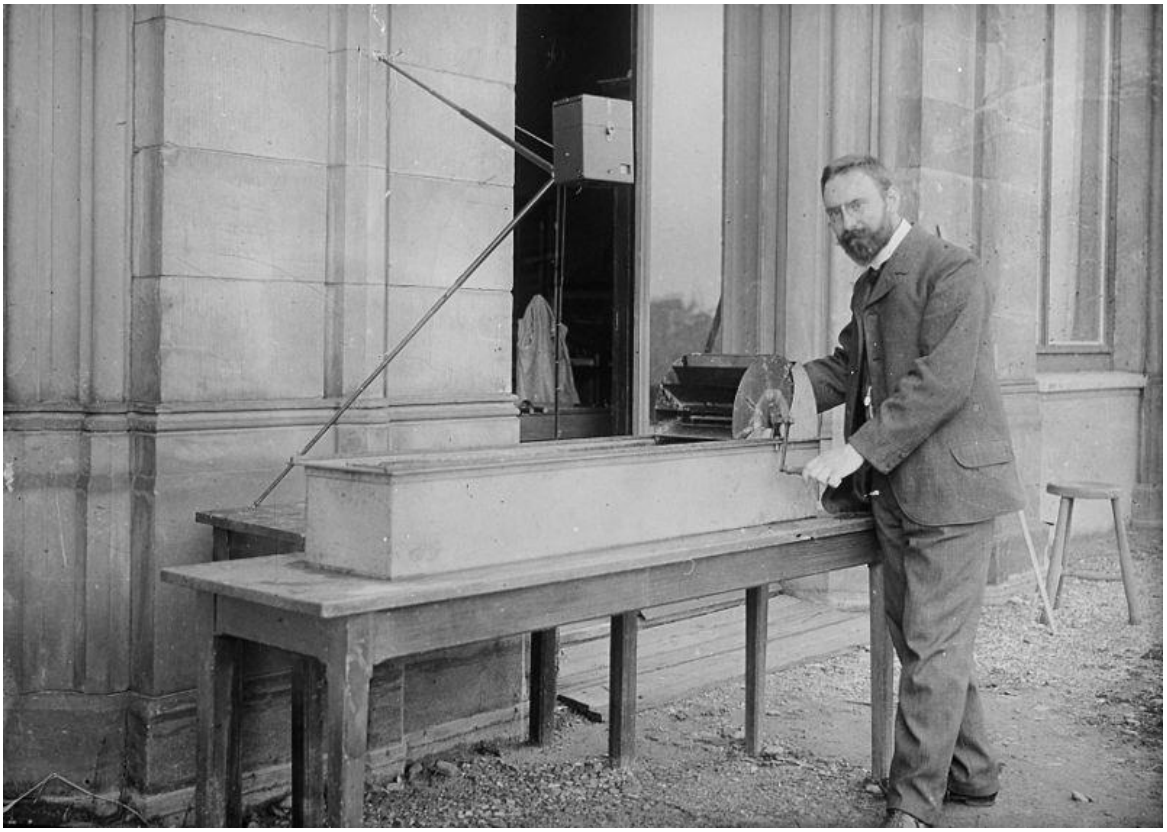

Figure 1: Ludwig Prandtl with his fluid test channel in 1904 [1].

With the increasing power of computers and widespread use of CCD cameras, non-invasive optical techniques have become fairly common. The development of lasers added another dimension to the field of flow visualization and provided a very powerful tool to study the flow dynamics. However, other particle tracking techniques like Radioactive Particle Tracking (RPT), Positron Emission Particle Tracking (PEPT), Magnetic Particle Tracking (MPT) and Passive Acoustic Emissions (AE) monitoring techniques have been developed since, each having their pros and cons. The assessment of the method of choice is done based on the physical problem and its constraints. Each of the above-mentioned methods are discussed briefly in the following chapter.

1.2.2 Particle Tracking Techniques

1.2.2.1 Optical Techniques

The earliest non-invasive optical techniques focused on the use of cameras to obtain videos and/or images of the vessel being studied which usually had a free surface or transparent wall. A few tracer particles were added to the granular material to study the trajectory of particles in the vessel. The vessel being studied usually had a transparent wall or free surface to allow for image acquisition as shown in *Figure 2*. Sometimes, instead of tracer particles, tracer zones were used. The tracer zones were composed of the same granular material as the bulk but with different colour. The tracer zones were disturbed and dispersed, as the blade moved, allowing the mixing mechanism to be studied.

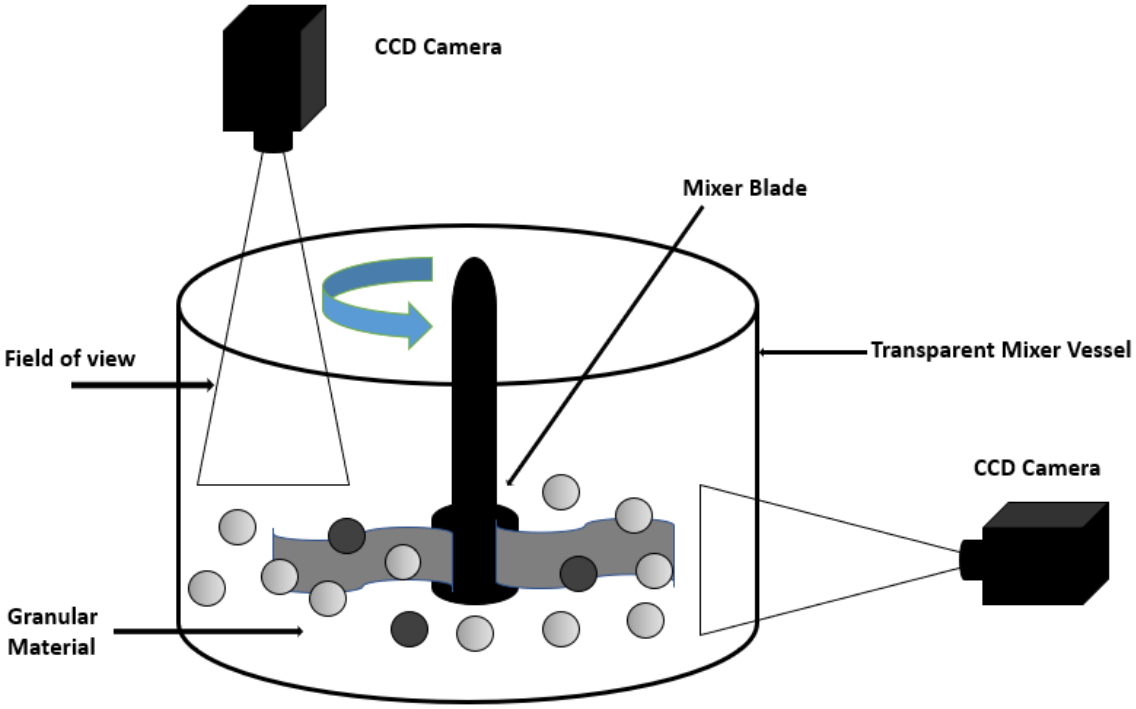

Figure 2: Typical optical image analysis setup, images are obtained at the transparent walls and top free surface.

Qualitative imaging techniques are low cost and well adapted for the preliminary investigation of granular mixing, surface phenomenon, flow regime transition and pattern formation. For example, mixing of glass beads and red oak chips in a transparent continuous screw mixer was investigated by Kingston and Heindel [3]. Four different cameras were employed at four different projections simultaneously to capture the entire periphery of the mixing process. The qualitative effects of rotation speed and screw pitch on mixing effectiveness and particle velocity were reported in the above-mentioned study. However, without post processing such as image analysis, much of the data regarding the flow mechanism like velocity profiles cannot be quantified. Therefore, the access to a transparent wall or free surface and extensive post-processing capabilities becomes necessary for such techniques.

Particle Image Velocimetry (PIV) makes use of the acquisition of consecutive images taken at known time difference which are then correlated to obtain displacement and velocity vectors of particles in the investigated regions [4]. The particle displacement between two consecutive images taken after a known time delay is used to calculate the particle velocity. In some cases, the investigated window is divided into smaller cells and the light intensity in a particular cell at an instant is cross correlated with the light intensity in neighbouring cells at another instant. Employing this method, the average movement of a group of particles can be obtained in the form of average particle displacement vectors [4]. A number of studies [4-8] were performed on vertical axis bladed mixers. High speed CCD cameras were used to acquire PIV data at the top free surface as well as the transparent walls. Effect of blade speed, moisture content, and particle roughness were reported in these studies.

Owing to the fact that the field of optics is highly mature, the equipment is simple and economical when compared to other techniques. The only constraint on the tracer particle, in most cases, is that it needs to be different from the bulk material and hence is easy to

manufacture. Optical techniques are inexpensive and thus can be used as ‘pre-experiments’ to validate the phenomenon before using advanced and expensive techniques. Optical methods have high spatial and temporal resolution.

The greatest limitation of the optical technique is that only wall or surface phenomenon can be investigated. Moreover, it is not always possible to have access to free surface or transparent walls. Sometimes, the tracer particle can get completely covered by the bulk material causing the location and velocity to not be recorded. The image processing can also get complicated due to the effect of reflection of light off the vessel walls and scratches on the wall which affect the image clarity. These limitations have prevented optical methods from gaining momentum as a technique to study granular flows.

1.2.2.2 Radioactive Particle Tracking Technique

In Radioactive Particle Tracking, the motion of a tracer particle designed to be the marker, whose velocity is to be mapped, is tracked. The tracer particle is normally a gamma ray emitter. The particle is made neutrally buoyant for tracking liquid phase; and for tracking granular solids, the size, shape and density of the tracer particle is matched to that of the granular material. An array of detectors is placed around the vessel to record the photon counts. The first level processing yields the Lagrangian position time series of the tracer particle. Secondary processing leads to Eulerian mean velocities, moments of velocity fluctuations, and other flow quantities. This information is used to quantify the fluid flow.

Radioactive particle tracking techniques have been well established and find extensive use in various medical fields. The RPT method makes use of the disintegration of a radioactive particle to track the location and velocity of the tracer particle in the mixer. Detectors are placed around the mixer vessel which detects the radioactive tracer as a function of position at a given instant of time and the emission history is recorded. A typical

RPT setup is presented in *Figure 3* with the data from the detectors being fed to software to reconstruct the path followed by the tracer. It is expected that these particles would follow the trajectory and velocity of the granular media inside the vessel. Radioactive isotopes with known decay rate and energy are used as they emit radiation in all directions that can be detected using a detector array. Chaouki et al. [9] discusses three different reconstruction methods to locate the tracer particle.

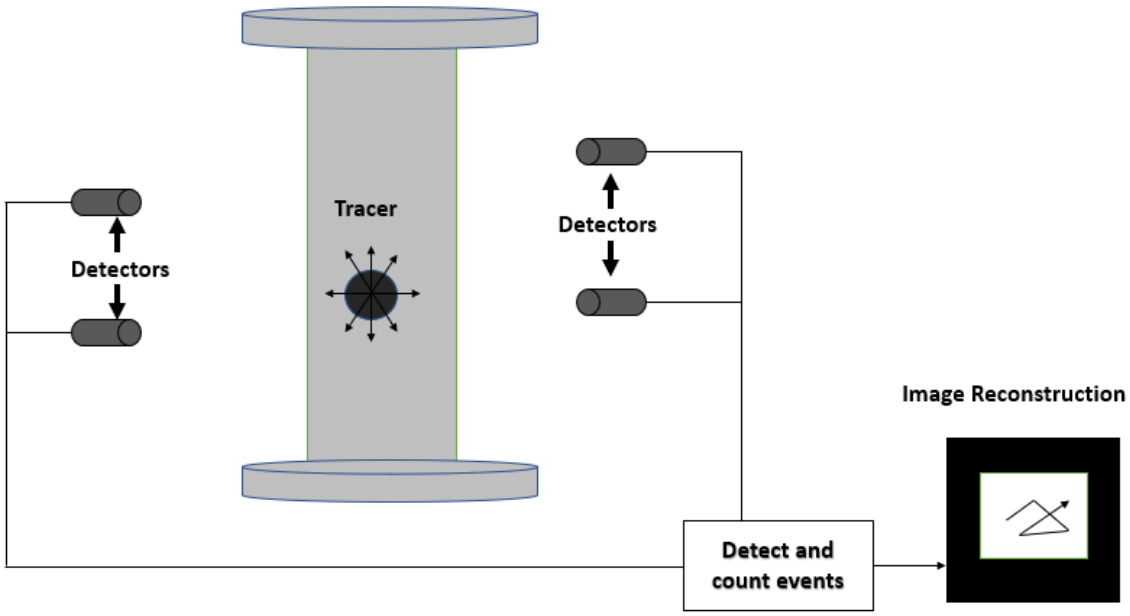

Figure 3: A typical radioactive particle tracking experiment, counts received by the detectors are used to reconstruct the location of the tracer particle over time. [2]

Roy et al. [10] discusses the strengths and limitations of RPT applied to a gas-solid riser. At least 3 detectors are needed on a single plane and they should be distributed evenly around the vessel. The greatest limitation, however, of RPT is that only a single particle can be tracked at a given time. Rasouli et al. [11] uses a multiple radioactive particle tracking (MRPT) technique to study the movement of cylindrical particles in a rotating drum.

RPT measurements are remarkably effective and have found extensive use in granular mixing characterization. The unique advantage of this technique is that the position and velocity of individual particles can be obtained. However, a major challenge with RPT and PEPT lies in optimal tracer path selection. The tracer particle should be able to follow the flow path line accurately. The radioactive strength and half-lives need to be selected appropriately along with meeting the safety requirements. Also, multiple detectors need to be placed along the entire length of the vessel which drives up the cost and complexity of the system. The detectors require careful calibration and optimization procedure before the detector can be employed in each new system. Moreover, RPT equipment is not standardized, requiring each system to be designed for the specific application at hand. Another significant limitation is that imaging multiple tracer particles within acceptable time frames is difficult to achieve. This limitation restricts capturing of particle-particle interactions which is a must for understanding of granular flows. This also implies that a smaller number of particles will require longer experiments to obtain meaningful data.

1.2.2.3 Positron Emission Particle Tracking Technique

Positron emission particle tracking is the most widely used radioactive particle tracking technique used in granular flows. A radioisotope is incorporated into a tracer particle which undergoes beta decay involving emission of a positron. Once emitted from the nucleus, the positron annihilates with an electron, releasing energy from the nucleus in the form of two 511keV gamma photons which are emitted back-to-back, 180^{o} apart to within 0.5^{o}. This setup is shown in *Figure 4*. The position of the trajectory on which the two photons lie can be determined if the position of both the photons can be detected [12]. If a line is drawn from the detection points of the coincident photons, the tracer particle would lie on this line which is called the Line of Response (LoR) [13]. Multiple LoRs should then intersect at the location of

tracer particle. The location of the particle is continuously tracked and a Lagrangian path and velocity of the tracer particle can be recreated, as it moves through the system.

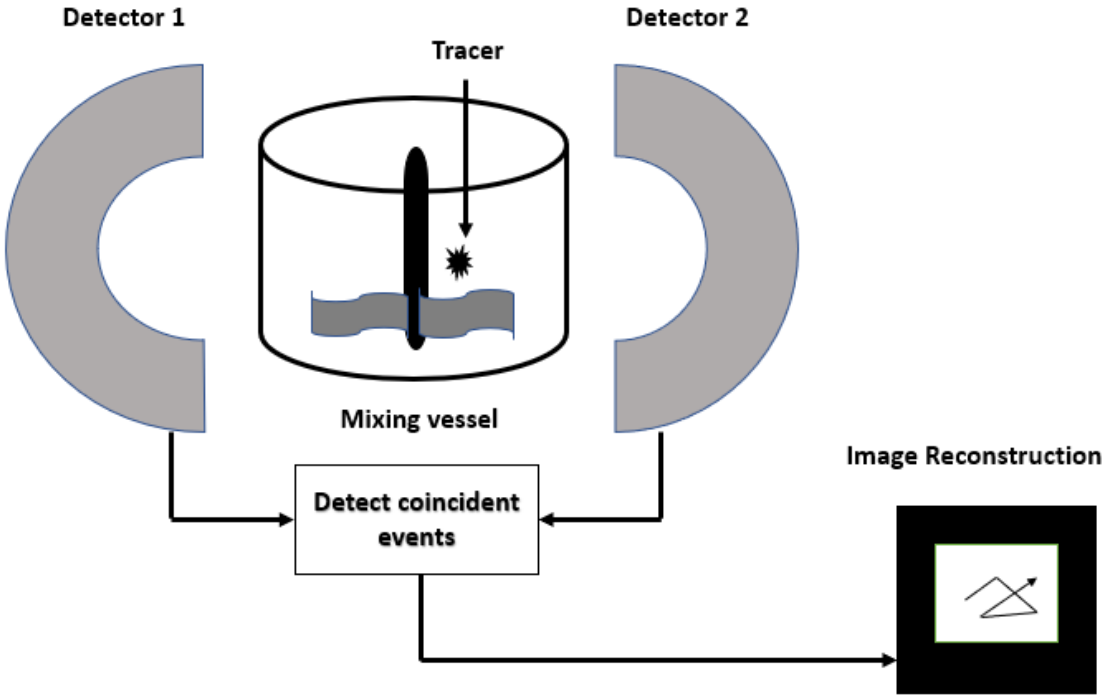

Figure 4: Detectors simultaneously detect the photon pair in a typical PEPT setup performed in a horizontal bladed mixer. [2]

A simplified yet faster version of the PEPT method is the 2D PEPI (Particle Emission Projection Imaging) that only takes into consideration gamma ray pairs that are incident perpendicular to the cameras' planes. PEPI is usually employed to study slow moving fluids, particles and slurries [14]. However, due to non-standardization and complicated equipment setup and detector deployment, the use of this technique is limited to laboratory and pilot scale applications. Another major disadvantage of this technique is that it is difficult to achieve images of multiple tracer particles within acceptable time frames. If multiple particles cannot be tracked then particle-particle interaction becomes difficult to be studied.

1.2.3 History of Magnetic Particle Tracking Technique

Diseases of gastrointestinal tract are important illnesses to be studied in the field of internal medicine. The observation of dynamic processes is important for intestinal diseases and the intestinal passage also has to be monitored for the remote release either of special agents designed for functional examinations or of drugs for application in specific regions of the gastrointestinal tract. In all these cases, monitoring of capsules during their passage through the gut is required. Conventional methods for dynamic investigations are not ideal. The PEPT and RPT methods discussed above carry the risk of radiation exposure. Optical techniques cannot be applied due to unavailability of free surface or transparent boundaries.

Therefore, to tackle the above problem, Weitschies et al [15] proposed a very advanced magnetic technique (1997, 1999) called Magnetic Marker Monitoring (MMM). These authors published excellent pictures of marker motions through gastrointestinal tracts with high temporal and spatial resolution. The corresponding technique, however, is rather complicated; the measurements have to be performed in a magnetically shielded room using multiple channel SQUID magnetometers and a specially designed data acquisition system. To improve on the above shortcoming, Andra et al [16], proposed the novel technique of Magnetic Particle Tracking in 2000. A significant advantage of this novel method is that it provides real-time monitoring in contrast to the above-mentioned technique described by Weitschies *et al* (1997, 1999).

In other early efforts, the MPT method was used to track large objects in dense gas fluidized bed with different densities and air flow rates [17-19]. Recently, Kohler et al. studied the mixing and segregation of fuel in a bubbling fluidized bed where they used the MPT method to determine the vertical distribution of the tracer in a down scaled cold unit [20,21]. Zhang et al [22] used MPT to measure the particle trajectory in a rotating drum.

1.2.4 Why MPT

Tracking an object's or a particle's motion is critical in the study of turbulent mixing, granular flow, sedimentation, and cellular biology [23-26]. Usually, the advanced particle tracking technologies are optical based (e.g. Lagrangian particle tracking) and some algorithms are suggested to improve the accuracy. They are of high precision; however, they can hardly be used in opaque multiphase flows or granular motions, and obtaining the object's rotational information takes a lot of effort [27,28]. Therefore, a group of nonintrusive tracking methods, which do not require optical accessibility, are developed. For instance, radioactive particle tracking (RPT) and positron emission particle tracking (PEPT), as discussed earlier, are used to obtain the kinetics of particles in a fluidized bed. The RPT directly uses the gamma radiation emitted in the beta-decay of a source particle. The PEPT uses radioactive material such as ^{18}F, ^{61}Cu, and ^{66}Ga to label a particle. These materials emit positrons, which annihilate with electrons and generate back-to-back gamma rays. The gamma rays can be monitored by gamma detectors, from which the position of the source can be determined. The PEPT is a variant of Positron Emission Tomography (PET). The PET generates an image while the PEPT uses a single particle as a labelled tracer. In addition, X-rays have also been used to measure motion in an opaque environment, such as air bubbles in gas-solid fluidized bed and gas-liquid reactors. The X-Ray applications in the visualization of multiphase flows is reviewed by Heindel and co-workers [3].

The RPT/PEPT requires the use of radioactive material while the Optical methods require a transparent wall or a free surface to be employed. In certain fields, these limitations prevent the use of the particle tracking techniques. To overcome this, Magnetic Particle Tracking (MPT) technique was introduced in the medical field by Weitschies and Andra [15,16] for examining the gastrointestinal tract without the risk of radiation exposure. Later,

the MPT was also used in chemical engineering, especially in the measurement in dense gas fluidized beds.

The MPT is capable of measuring the particle orientation, which is called the magnetic moment direction. The working principle of MPT is very simple. The field of a small magnet can be modelled as a dipole field uniquely determined by the magnet's position and orientation. Based on the field strength at multiple locations measured by a set of magnetometers, it is possible to reconstruct the magnetic field and to consequently locate the magnet source. Therefore, both the translational and rotational motions of the magnetic particle are obtained simultaneously. This gives MPT a major advantage over the other techniques discussed earlier, since it is very difficult to get rotational motion using the optical based methods and impossible using the RPT/PEPT techniques. Also, when compared with other non-invasive techniques, the MPT only requires a set of magnetometers and a magnetic particle. Therefore, the cost of operation and setup is also significantly inexpensive with MPT as compared to RPT, PEPT and other optical based tracking techniques. The MPT setup, in addition, possesses no hazardous radiation threats. The advantages and disadvantages of prior techniques are summarized in *Table 1*.

Table 1: Pros and cons of the commonly used particle tracking techniques.

Method	**Optical -based methods**	**RPT/PEPT/X-rays**	**MPT**
Cost	Expensive	Very Expensive	Inexpensive
Working condition	Transparent only	Transparent or opaque	Transparent or opaque
Safety Requirement	Laser operation	Radiation protection	None
Spatial Resolution	High	Relatively low	Relatively low
Rotational motion	Difficult	Generally, no	Yes

1.2.5 Applications of MPT

The Magnetic Particle Tracking (MPT) technique is based on a basic principle and gives both the orientation and position of the tracer particle. It only requires a set of magnetometers and a magnetic particle and is therefore inexpensive compared to other techniques. This gives MPT a major advantage over the other techniques. A few major areas of applications include:

- In the study of granular flows.
- In the Medical field to study gastrointestinal tract.
- In the field of Geology to study sedimentation.
- In the field of Chemistry to study turbulent mixing.

1.3 Contribution and organization

The major contribution of this thesis includes:

- Development of a Magnetic Particle Tracking algorithm using a Hybrid Numerical Optimization Method that tracks both the particle's position and orientation simultaneously in 3D. This algorithm is comparable in accuracy with the state-of-the-art techniques available in literature but is orders of magnitude faster.
- Provides a powerful tool for studying dense granular flows which provides valuable insights into this physical phenomenon.

The organization of this thesis is as follows. The chapter 1 described the history of particle tracking and also describes the most popular particle tracking techniques used in literature. This chapter also included the history of MPT and described advantages of MPT over the other particle tracking techniques. In chapter 2, the 2D analytical solution of the MPT problem is described. It details the need for a numerical solution to the problem. It is followed by the description of the popular optimization methods available in literature. The Hybrid Numerical Optimization algorithm proposed in this work is described in detail and the procedure to use it are outlined in chapter 3. In chapter 4, certain special numerical simulations are tested with the MPT algorithm proposed to validate the results. The relative position and orientation error using the Hybrid Numerical Method is then compared with the other optimization techniques and the results are summarized. In chapter 5, the importance of granular shear flow is discussed and how MPT can be used to study these flows is described. The experimental setup and the results are discussed in detail in this chapter. Chapter 5 and 6 outlines the conclusions and recommendations for future work on this topic.

2. Analytical Solution

2.1 Introduction

This chapter provides the 2D analytical solution to the single particle tracking setup using Magnetic Particle Tracking (MPT) technique. It details how analytically the particle's position and orientation can be reconstructed based on the measured magnetic signals. The principle of the MPT measurement technique relies on tracking of a single magnetic marker. Evaluation of the quasistatic magnetic field results in a position estimate. This is an inverse problem with five degrees of freedom, three for position and two for orientation. When the magnetic moment of the marker is unknown this can act as a sixth degree of freedom. The magnetic field is measured by several sensors that are positioned in a known configuration. The theoretical signals are calculated using the derivation of a magnetic field of a magnetic dipole at sufficient distance from the dipole. Therefore, theoretically we should be able to reconstruct both the particle's position and orientation.

2.2 Basic Definitions

i. Magnetic dipole

Magnetic dipole is, generally a tiny magnet of microscopic to subatomic dimensions, equivalent to a flow of charge around a loop. Electrons circulating around atomic nuclei, electrons spinning on their axes, and rotating positively charged atomic nuclei, all are magnetic dipoles. The sum of these effects may cancel so that a given type of atom may not be a magnetic dipole. If they do not fully cancel, the atom is a permanent magnetic dipole, as are iron atoms. Many millions of iron atoms spontaneously locked into the same alignment to form a ferromagnetic domain also constitute a magnetic dipole. Magnetic compass needles and bar magnets are examples of macroscopic magnetic dipoles.

ii. Magnetic dipole moment

The strength of a magnetic dipole, called the magnetic dipole moment, may be thought of as a measure of a dipole's ability to turn itself into alignment with a given external magnetic field. In a uniform magnetic field, the magnitude of the dipole moment is proportional to the maximum amount of torque on the dipole, which occurs when the dipole is at right angles to the magnetic field. The magnetic dipole moment, often simply called the magnetic moment, may be defined then as the maximum amount of torque caused by magnetic force on a dipole that arises per unit value of the surrounding magnetic field in vacuum. It is measured in unit $A.m^2$.

iii. Magnetic flux density

The magnetic field can be defined in several equivalent ways based on the effect it has on its environment. The magnetic field is often described by the force it exerts on a charged particle. A vector quantity measuring the strength and direction of the magnetic field around a magnet or an electric current is called the magnetic flux density. Magnetic flux density is equal to magnetic field strength times the magnetic permeability in the region in which the field exists. Magnetic flux density can also be understood as the density of magnetic lines of force passing through a specific area. It is measured in unit Tesla.

iv. Magnetic permeability

Magnetic permeability is the relative increase or decrease in the resultant magnetic field inside a material compared with the magnetizing field in which the given material is located; or the property of a material that is equal to the magnetic flux density B established within the material by a magnetizing field divided by the magnetic field strength H of the magnetizing field. Magnetic permeability μ is thus defined as,

$$\mu = \frac{B}{H} \quad (1)$$

Magnetic flux density *B* is a measure of the actual magnetic field within a material considered as a concentration of magnetic field lines, or flux, per unit cross-sectional area. Magnetic field strength *H* is a measure of the magnetizing field produced by electric current flow in a coil of wire.

In empty, or free, space the magnetic flux density is the same as the magnetizing field because there is no matter to modify the field. In CGS units, the permeability *B*/*H* of space is dimensionless and has a value of 1. In MKS and SI units, *B* and *H* have different dimensions, and the permeability of free space (symbolized μ_0) is defined as equal to $4\pi \times 10^{-7}$ weber per ampere-metre so that the MKS unit of electric current may be the same as the practical unit, the ampere. In these systems the permeability, *B*/*H*, is called the absolute permeability μ of the medium. The relative permeability μ_r is then defined as the ratio μ/μ_0, which is dimensionless and has the same numerical value as the permeability in the CGS system. Thus, the relative permeability of free space, or vacuum, is 1.

Materials may be classified magnetically on the basis of their permeabilities. A diamagnetic material has a constant relative permeability slightly less than 1. When a diamagnetic material, such as Bismuth, is placed in a magnetic field, the external field is partly expelled, and the magnetic flux density within it is slightly reduced. A paramagnetic material has a constant relative permeability slightly more than 1. When a paramagnetic material, such as platinum, is placed in a magnetic field, it becomes slightly magnetized in the direction of the external field. A ferromagnetic material, such as iron, does not have a constant relative permeability. As the magnetizing field increases, the relative permeability increases, reaches a maximum, and then decreases. Purified iron and many magnetic alloys have maximum relative permeabilities of 100,000 or more.

2.3 2D Analytical Solution

In a simple setup, *Figure 5*, we can analytically reconstruct the particle's position and orientation based on the measured magnetic signal. This setup includes two 3-axis magnetometers located at Point 0 and 1 with $\boldsymbol{x}_0 = (0, 0, 0)$ and $\boldsymbol{x}_1 = (L, 0, 0)$. They, together provide 6 signals (B_{0x}, B_{0y}, B_{0z}) and (B_{1x}, B_{1y}, B_{1z}).

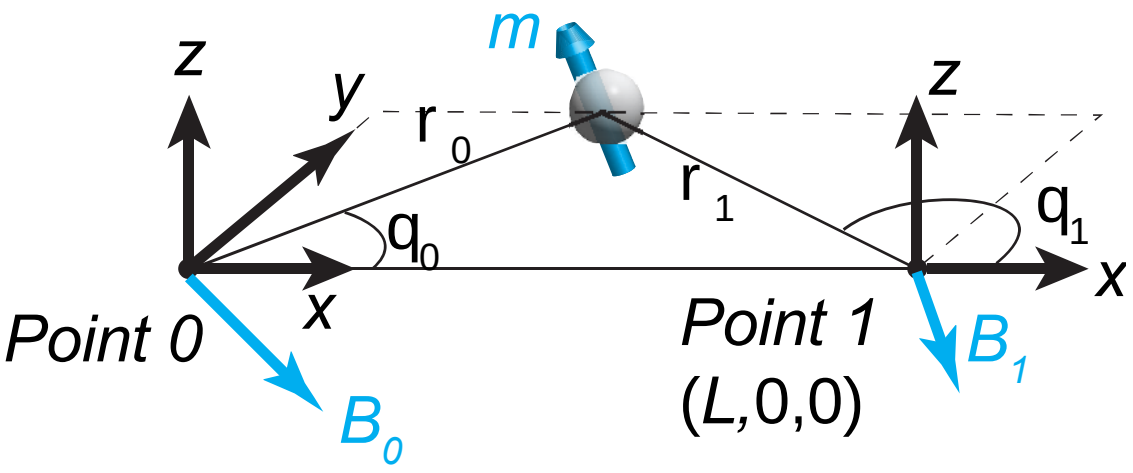

Figure 5: A simple magnetic particle tracking setup

The magnetic field of the particle is described by a dipole as,

$$B(x_{0,1}) = \frac{\mu_0}{4\pi}\frac{[3n \cdot (m \cdot n) - m]}{|x - x_{0,1}|^3} \tag{2}$$

where $\boldsymbol{x}$ is the magnet's location, $\boldsymbol{n}$ is the normal vector in the $\boldsymbol{x} - \boldsymbol{x}_i$ direction (i = 0 or 1), and $\boldsymbol{m}$ is the magnetic moment, μ_0 is the magnetic permeability. The position of the magnet can be found analytically based on equation (2). The flowchart shown in Figure *6* describes the logic used to solve the above equation. The proper derivation of the solution is described later.

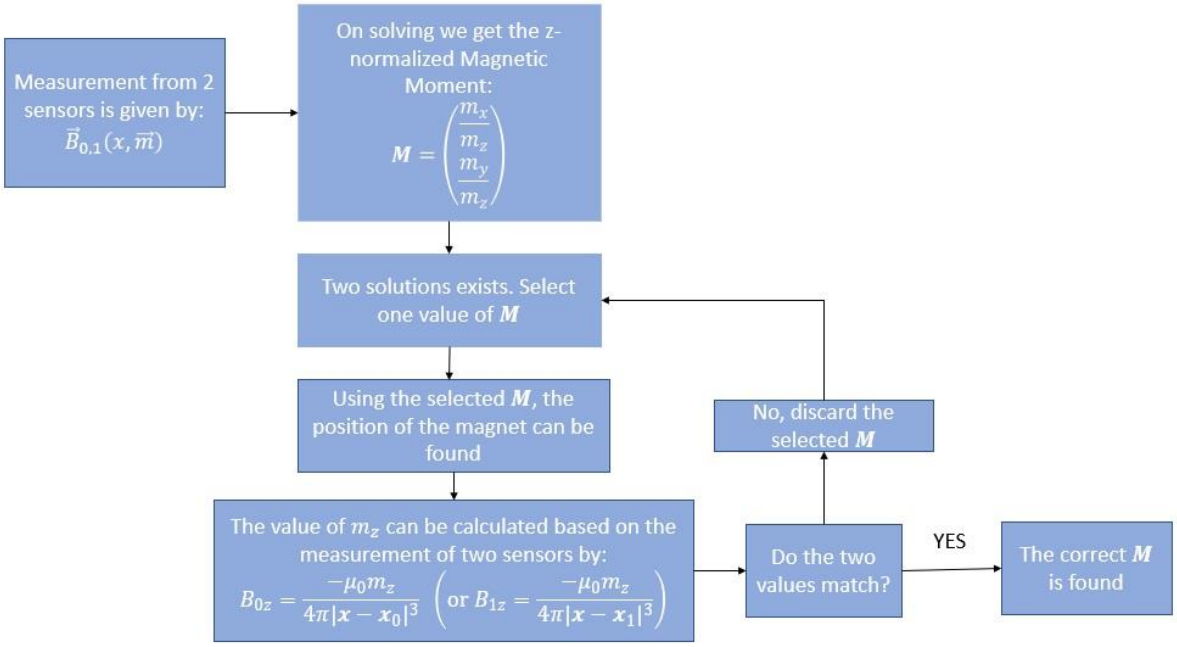

Figure 6: Flowchart describing the 2D Analytical solution

The dipole field is exact for a uniform spherical magnetic bead, and it is a very good approximation for the far field of non-spherical beads. The frame of reference is constructed such that the magnetic particle is on the *XY* plane (*Figure 5*). Therefore, $\boldsymbol{x} - \boldsymbol{x}_i$ lies on the *XY* plane and $\boldsymbol{n}_i = (n_{ix}, n_{iy}, 0)'$. The magnetic field equation becomes,

$$\begin{pmatrix} B_{ix} \\ B_{iy} \\ B_{iz} \end{pmatrix} = \frac{\mu_0}{4\pi|\boldsymbol{x}-\boldsymbol{x_i}|^3} \begin{pmatrix} 3n_{ix}(m_x n_{0i} + m_y n_{iy}) - m_x \\ 3n_{iy}(m_x n_{ix} + m_y n_{iy}) - m_y \\ -m_z \end{pmatrix} \tag{3}$$

The problem is to calculate $\boldsymbol{m}$ and $\boldsymbol{x}$ based on the measured $\boldsymbol{B}$s. Here we need to define some new variables:

$T_i = (T_{ix}, T_{iy})$, where $T_{ix} = \frac{B_{ix}}{B_{iz}}$ and $T_{iy} = \frac{B_{iy}}{B_{iz}}$

Therefore, we get:

$$T_i = \begin{bmatrix} \frac{B_{ix}}{B_{iz}} \\ \frac{B_{iy}}{B_{iz}} \end{bmatrix} = -(3n\,.\,(M\,.\,n) - M) \tag{4}$$

where, *M* is the z-normalized magnetic moment ratio written as,

$$M = \begin{bmatrix} \frac{m_x}{m_z} \\ \frac{m_y}{m_z} \end{bmatrix} \tag{5}$$

Now to get the 2D solution, we consider two sensors as shown in *Figure 5*. The two sensors, sensor 0 and sensor 1, are length *L* m. apart.

On multiplying equation (4) by $\hat{n}$, we get:

$$\hat{n}\,.\,\vec{T} = -2\hat{n}\,.\,\overrightarrow{M} \tag{6}$$

Therefore, on solving equation (6), we have,

$$(T + 2M)\begin{bmatrix} cos\theta \\ sin\theta \end{bmatrix} = 0 \tag{7}$$

Therefore, on expanding the above equation, we have

$$(T_x + 2M_x)cos\theta + \left(T_y + 2M_y\right)sin\theta = 0 \tag{8}$$

Dividing equation (8) throughout by *cosθ*, we have,

$$(T_x + 2M_x) + \left(T_y + 2M_y\right)tan\theta = 0 \tag{9}$$

Similarly, on multiplying equation (4) by $\widehat{n_z}$, we get

$$\widehat{n_z}\,.\,T = \widehat{n_z}\,.\,M \tag{10}$$

On expanding the above equation, we have,

$$(T - M)\begin{bmatrix} -sin\theta \\ cos\theta \end{bmatrix} = 0 \tag{11}$$

Therefore, on expanding, we have,

$$(T_x - M_x)sin\theta - (T_y - M_y)cos\theta = 0 \quad (12)$$

Dividing equation (12) throughout by *cosθ*, we have,

$$(T_x - M_x)\frac{sin\theta}{cos\theta} - (T_y - M_y) = 0 \quad (13)$$

On rearranging the above equation, we get,

$$tan\theta = \left(\frac{T_y - M_y}{T_x - M_x}\right) \quad (14)$$

Therefore, on substituting the above equation (14) in equation (9), we get:

$$(T_x + 2M_x) + (T_y + 2M_y)\left(\frac{T_y - M_y}{T_x - M_x}\right) = 0 \quad (15)$$

$$(T_x + 2M_x)(T_x - M_x) + (T_y + 2M_y)(T_y - M_y) = 0 \quad (16)$$

$$(T_x^2 - T_xM_x + 2M_xT_x - 2M_x^2) + (T_y^2 - T_yM_y + 2M_yT_y - 2M_y^2) = 0 \quad (17)$$

Divide by 2 throughout, we have:

$$\left(\frac{8}{16}T_x^2 - \frac{1}{2}T_xM_x + M_xT_x - M_x^2\right) + \left(\frac{8}{16}T_y^2 - \frac{1}{2}T_yM_y + M_yT_y - M_y^2\right) = 0 \quad (18)$$

Now, the above equation can be split and written as,

$$\left(-\frac{1}{16}T_x^2 + \frac{9}{16}T_x^2 + \frac{1}{2}T_xM_x - M_x^2\right) + \left(-\frac{1}{16}T_y^2 + \frac{9}{16}T_y^2 + \frac{1}{2}T_yM_y - M_y^2\right) = 0 \quad (19)$$

On collecting all T_x and T_y terms on the LHS and rewriting the above equation, we get,

$$\frac{9}{16}(T_x^2 + T_y^2) = \left(M_x^2 - 2\,\frac{1}{4}\,M_xT_x + \frac{1}{16}\,T_x^2\right) + (M_y^2 - 2\,\frac{1}{4}\,M_yT_y + \frac{1}{16}\,T_y^2) \quad (20)$$

$$\frac{9}{16}(T_x^2 + T_y^2) = \left(M_y - \frac{1}{4}\,T_x\right)^2 + \left(M_y - \frac{1}{4}\,T_y\right)^2 \quad (21)$$

Observe that the above equation is of the form:

$$(x - h)^2 + (y - k)^2 = r^2 \quad (22)$$

which is the equation of a circle with the centre being at point *(h,k)* with a radius *r*.

Therefore, this suggests that we will have two analytical solutions to our problem. Just as from the sensor 0, we will have a similar equation from the sensor 1.

To solve the above system of equations, we define:

1) $\boldsymbol{T}_i = (T_{ix}, T_{iy})$, where $T_{ix} = \frac{B_{ix}}{B_{iz}}$ and $T_{iy} = \frac{B_{iy}}{B_{iz}}$;

2) $D = T_{1y}^2 - T_{0y}^2 + T_{1x}^2 - T_{0x}^2$;

3) $E = \frac{(T_{0x}T_{1y} - T_{1x}T_{0y})}{4}$; and

4) $S = \frac{1}{2}\left[T_{0x}^2 + T_{1x}^2 + T_{0y}^2 + T_{1y}^2 + (T_{0x} + T_{1x})M_x^* - 4M_x^{*2} + \left(T_{0y} + T_{1y}\right)M_y^* - 4M_y^{*2}\right]^{1/2}$.

They can be calculated once $\boldsymbol{B}$s are known. Then the z-normalized magnet moment $\boldsymbol{M} = (M_x, M_y) = (m_x/m_z, m_y/m_z)'$ can be obtained using these known variables. It is given as:

$$\boldsymbol{M} = \begin{pmatrix} \frac{m_x}{m_z} \\ \frac{m_y}{m_z} \end{pmatrix} = \begin{pmatrix} M_x^* \\ M_y^* \end{pmatrix} \pm \frac{S}{\sqrt{(T_{0x} - T_{1x})^2 + \left(T_{0y} - T_{1y}\right)^2}} \begin{pmatrix} T_{0y} - T_{1y} \\ -T_{0x} + T_{1x} \end{pmatrix} \quad (23)$$

where,
$$M_x^* = \frac{(T_{0x} - T_{1x})D - \left(T_{0y} - T_{1y}\right)E}{(T_{0x} - T_{1x})^2 + \left(T_{0y} - T_{1y}\right)^2} \quad (24)$$

and
$$M_y^* = \frac{\left(T_{0y} - T_{1y}\right)D + (T_{0x} - T_{1x})E}{(T_{0x} - T_{1x})^2 + \left(T_{0y} - T_{1y}\right)^2} \quad (25)$$

There are two solutions, and one of them is true. To proceed, selecting one $\boldsymbol{M}$, we can obtain,

$$\tan\theta_0 = \frac{\left(T_{0y} - M_y\right)}{T_{0x} - M_x} \quad (26)$$

and
$$\tan\theta_1 = \frac{T_{1y} - M_y}{T_{1x} - M_x} \quad (27)$$

Here θ_i is the angle between n_i and the x-axis. Consequently, the magnet's position is,

$$x = \frac{L\ tan\theta_1}{tan\theta_1 - tan\theta_0} \tag{28}$$

and $$y = \tan\theta_0 \cdot x. \tag{29}$$

Thereafter, the *z*-component equation is,

$$B_{0z} = \frac{-\mu_0 m_z}{4\pi|\boldsymbol{x} - \boldsymbol{x}_0|^3} \left(\text{or } B_{1z} = \frac{-\mu_0 m_z}{4\pi|\boldsymbol{x} - \boldsymbol{x}_1|^3}\right) \tag{30}$$

provides m_z, and $(m_x, m_y)' = m_z \cdot \boldsymbol{M}$.

If the selected $\boldsymbol{M}$ is wrong, the two m_z's calculated using B_{0z} and B_{1z} do not match and this $\boldsymbol{M}$ solution should be discarded. Therefore, once the correct $\boldsymbol{M}$ is known, we can get the exact location of the particle in the XY plane and also, it's orientation in that plane.

3. Computational Algorithm

3.1 Introduction

To reconstruct the particle position and orientation in 3D we have to rely on numerical methods. Equation (2) gives us the magnetic field measured by various sensors in a known configuration. Since a magnetometer usually measures the field component in a particular direction S, the senor observation should be $B.S$, i.e., the data from the i-th sensor should be,

$$D_i = B(x, x_{0i}, m).S_i \tag{31}$$

where i = 1, 2, 3,…, N and N is the total number of sensors. The real observation O from a sensor is generally different from the value D since it contains measurement noise which is about less than 5% for a typical magnetometer.

Since the position and direction of the sensor can be calibrated accurately, x_i and S_i are known. The task of MPT is to solve Equation (31) and determine the unknown variables x and m using a set of measured signals. The total degree of freedom (DOF) for the magnet is 6. But, if the total magnetic moment of the ball is measured in advance, the DOF reduces to 5. Therefore, at least five independent signals are needed to determine the magnetic field. In reality, the strength of a magnetic field decays as $|x - x_0|^{-3}$; hence, the signal will be very weak if the magnet is far from the sensor. To guarantee that the signal-to-noise ratio is high enough, in the following simulations and experiments, we use an array of four 3-axis probes to cover the entire measurement domain. The total number of signal channels are 12. For an arbitrary sensor arrangement, Equation (31) has no simple analytical solution. Therefore, the task becomes an optimization problem. Some of the popular and most recent optimization techniques used in literature have been discussed below.

3.2 Non-linear Optimization Techniques

Hu et al. [31] have studied several optimization algorithms among which a linear function is used for the initial guess and then several nonlinear optimization methods to determine the optimum are analysed. They found the Levenberg–Marquardt (LM) algorithm [31] to be both fast and accurate. They concluded that the LM method provides satisfactory tolerance for initial guess parameters, negligible computation error when the error level of the initial guess is within some threshold (position error within 20 cm), and fast speed (<0.11 s in MATLAB). In the LM algorithm, the solution of Equation (2) is done by solving for the positions x, y, z and the angles β, θ. Because β is periodic, estimates across this periodic boundary, 180 to -180, are difficult to solve and result in erroneous solutions [31].

Later, Buist et al. [32,33,34] used the Sequential Quadratic Programming (SQP) algorithm to determine the position and orientation of the particle by comparing the theoretical signal strength (S_t), which is the multiplication of magnetic field with the orientation of the senor, with the actual signal given by 72 sensors (S_m). The difference between the two is minimized using a quality function given by,

$$Q = \sum_{i=1}^{72} \frac{\left(\left(S_{m,i} - \langle S_m \rangle\right) - \left(S_{t,i} - \langle S_t \rangle\right)\right)^2}{\Delta S_{m,i}^2} \tag{32}$$

Gradient-search methods like the LM [31] and SQP [32,33,34] algorithms, need an initial estimate to converge to a local minimum. At the beginning of the analysis, the algorithm is initialized using a multistart method, a functionality in MATLAB. This multistart method uses multiple starting positions to find the global minimum. For any consecutive time-step, the previous time step is used as an initial estimate. However, if the algorithm is unable to converge or the quality function is too high, the algorithm is set to reinitialize. Therefore, by principle if the algorithm finds its minimum on the boundary/constraint of the setup, this solution must be seen as erroneous and the algorithm is also set to reinitialize. Any final

solution at the physical constraints is seen as an outlier. However, the cost function in the optimization is highly nonlinear and possesses many local minima. Hence, the reconstruction, which aims to find the global minimum, is time consuming. Therefore, the SQP algorithm solves a sequence of subproblems that optimizes a quadratic model of the quality function.

A new development in MPT technology was recently proposed by Tao et al. [29,30] in which two new reconstruction methods were developed using the extended Kalman filter (EKF [35,36]) and Sequential Importance sampling with Resampling (SIR [37,38]). These two methods are based on the reformulation of the MPT as a state space model, commonly used in science and engineering to define the state of a system from an unpredictable model augmented by a stream of noisy data. In the state space model, the state of the system is regarded as a stochastic process, and its conditional probability distribution is approximated based on the given data. The conditional mean will give the minimum mean square error estimation of the state, and the uncertainty is given by the covariance. If the model and the observation function are both linear and the noises (in the model and observation) are Gaussian, the Kalman filter will measure the conditional mean and covariance [39,40]. The EKF is an extension of the Kalman filter. It can handle complex dynamics and nonlinear observation functions, but the noises in both model and observation are still assumed to be Gaussian. The SIR is one of the particle filters [37,38] which can be used for general nonlinear non-Gaussian situations.

In the EKF algorithm, the state variable, $X_k = \binom{r_k}{m_k}$, represents the particle status at time step *k*. The state variable at step *k* is modelled based on the particle status at step *k-1*. The location of the particle r_k is based on its position and velocity and hence can be modelled by the kinematic equation. Similarly, the rotation of the magnetic particle can be modelled using a quaternion. This in addition with the observation equation (O_k), form a state-space model. The mean of the conditional probability distribution of the state X_k given the

measurement O_k gives the mean square error estimate of the state X_k, while the uncertainty is given by the covariance of the conditional probability distribution. Now, specifically for the EFK algorithm, the conditional probability distribution is approximated by a Gaussian distribution. In the SIR method, the conditional probability distribution of the state variable of the entire trajectory is presented by a set of samples with associated weights. It was concluded using numerical experiments that EKF provides same accuracy as SQP, but it was orders of magnitude faster. The efficiency of SIR was between that of the EKF and SQP.

In this work, we present a Hybrid Numerical Optimization Method for single particle tracking. In this method, the local minimization begins with an initial estimation and follows the fastest gradient direction to search for the local minimum. In practice, we combine global and local minimization algorithms to find the best $\boldsymbol{x}$ and $\boldsymbol{m}$.

3.3 Hybrid numerical method for single particle tracking

As discussed earlier, in a complex 3D setup with multiple sensors, there is no analytical solution. We resort to numerical methods to calculate the magnet's position and orientation. The main idea is to find the best $\boldsymbol{x}$ and $\boldsymbol{m}$ minimizing this function:

$$\Phi = \sum_i (P_i(\boldsymbol{B_i}) - Q_i)^2 \tag{33}$$

in which $\boldsymbol{B_i} = \boldsymbol{B_i}(\boldsymbol{x}, \boldsymbol{m})$ is the magnetic field at the location of the i-th sensor. Φ measures the difference between the sensor reading Q_i and the theoretical field intensity generated by a magnetic dipole $\boldsymbol{m}$ located at $\boldsymbol{x}$. P_i is a function depending on the sensor: if the sensor measures one component, $P_i = \boldsymbol{s} \cdot \boldsymbol{B}_i$, i.e., the component along the sensor direction $\boldsymbol{s}$; and if it measures the magnitude, $P_i = | \boldsymbol{B}_i |$.

In practice, we combine global and local minimization algorithms to find $\boldsymbol{x}$ and $\boldsymbol{m}$. The local minimization begins with an initial estimation and follows the fastest gradient direction to search for the local minimum. At the beginning of one trajectory, there is no

accurate estimation for $\boldsymbol{x}$ or $\boldsymbol{m}$. Thus, global optimizations, such as the gradient method, can provide the desired results. After some time, a short trajectory can be constructed. We can, subsequently, estimate the position at next step based on the previous trajectory. This estimation is used as the beginning point in local minimization. The hybrid method saves considerable computation time.

The position and orientation reconstruction accuracy of this algorithm is tested in the next chapter using several general synthetic numerical simulation cases. This method is then compared and analysed with the SQP, EKF and SIR algorithms discussed earlier.

4. Numerical simulation

4.1 Introduction

The MPT algorithm described in chapter 3 should be able to track a single particle's position and orientation in 3D. In this section, we test the performance of the algorithm in common scenarios using numerical simulations. We use several simulations to evaluate the performance of the algorithm in the reconstruction of the trajectories. The cases that will be studied in this section are continuous velocity and acceleration, sudden change in orientation, sudden change in position and then the Brownian motion simulation. The study of Brownian motion is crucial since if the algorithm can track a particle trajectory following Brownian motion, then the algorithm can be used in any situation for the trajectory reconstruction. To evaluate the robustness of the algorithm, Gaussian noise is added to the synthetic sensor readings and then the accuracy is analysed.

4.2 Smooth trajectory with continuous velocity

Here we simulate a particle motion in 3D with continuous velocity and with no change in the orientation. The normalized magnetic moment is set to be 0.01 Am^2. In this case, only the x-component of velocity changes with respect to time while the y and z-component remain constant. The position vector for the above case is given by:

$$\vec{r} = 0.5\, t\, \hat{\imath} + 0.5\, \hat{\jmath} + 0.5\, \hat{k} \tag{34}$$

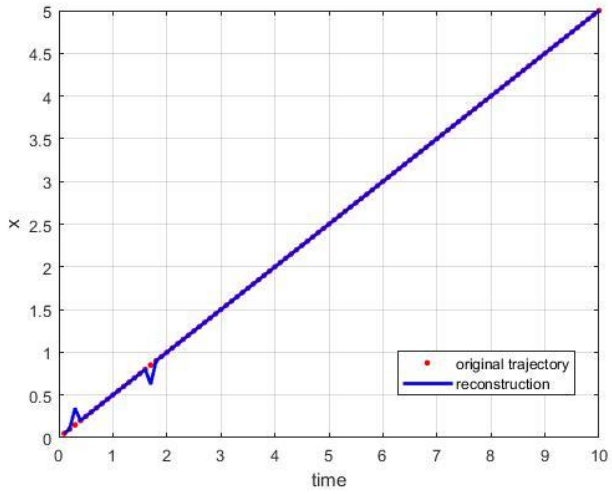

Figure 7: The x component particle reconstruction using the hybrid numerical method algorithm for continuous velocity simulation (no noise)

Figure 7 shows the reconstruction of the particle trajectory in the x-direction with respect to time and compares it with the original trajectory. The total time step is 1000, but only a section is presented for clarity. It can be observed that the MPT algorithm is able to reconstruct the particle position accurately for this case. The measurement in an actual experimental setup will contain some degree of noise. Therefore, we add 3% gaussian noise to the synthetic sensor readings and test the performance of the reconstruction. It can be seen in Figure 8 that the MPT is able to reconstruct the particle location relatively well even with the noise in the measurement. Generally, the error in the magnetometer reading does not exceed 5% of the actual measurement. Therefore, the reconstruction of the trajectory shown below should be acceptable in an actual experimental setup.

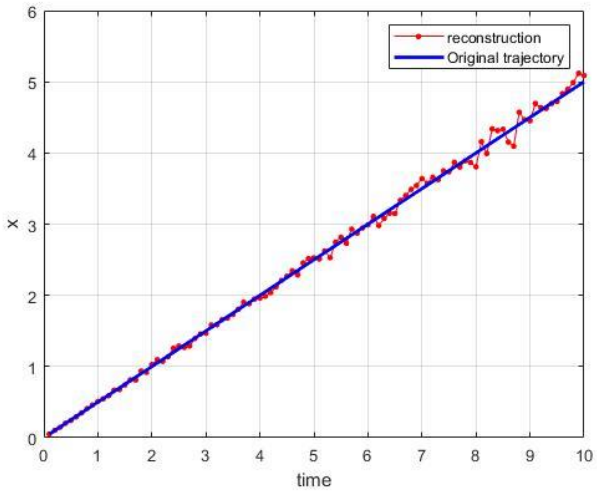

Figure 8: The x component particle reconstruction using the hybrid numerical method algorithm for continuous velocity simulation (3% noise)

4.3 Smooth trajectory with continuous acceleration

Here, we simulate a particle in 3D with continuous acceleration and with no change in the orientation. The normalized magnetic moment is set to be 0.01 Am^2. In this case, only the x-component of the acceleration change with respect to time while the y and z-component remain constant. The position vector for the above case is given by:

$$\vec{r} = 0.5\, t^2\, \hat{\imath} + 0.5\, \hat{\jmath} + 0.5\, \hat{k} \tag{35}$$

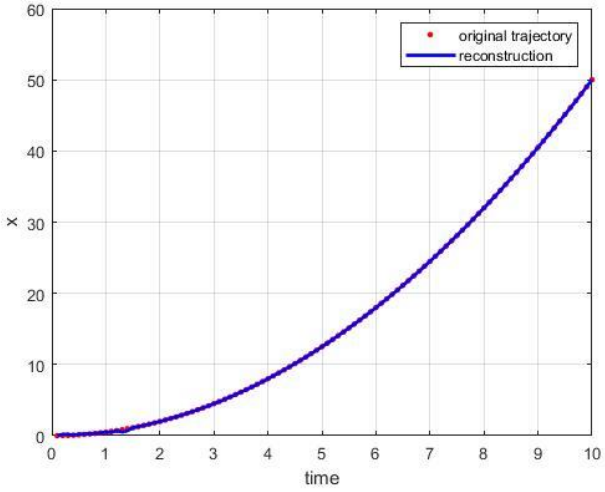

Figure 9: The x component particle reconstruction using the hybrid numerical method algorithm for continuous acceleration simulation (no noise)

Figure 9 shows the reconstruction of the particle trajectory in the x-direction with respect to time and compares it with the original trajectory. The total time step is 1000, but only a section is presented for clarity. Just like in the previous case, 3% gaussian noise is added to the synthetic sensor readings and the reconstruction performance is tested. *Figure 10* shows that the algorithm copes well with the continuous acceleration simulation with noisy data.

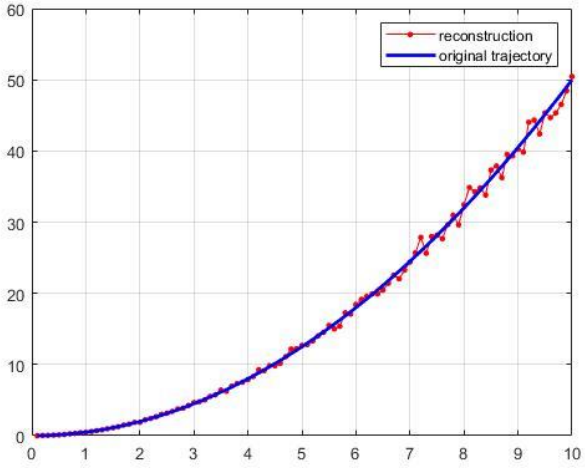

Figure 10: The x component particle reconstruction using the hybrid numerical method algorithm for continuous acceleration simulation (3% noise)

4.4 Sudden change in position and orientation

It will be interesting to see how the code performs when there is sudden change in direction and the orientation of the particle. The particle is simulated to change the x, y and z position at regular interval of time while keeping the particle orientation to be a constant. The normalized magnetic moment is set to be 0.01 Am^2. The results of the reconstruction are shown in Figure 11.. It can be seen that algorithm manages to track the particle accurately even with the sudden changes in the position over a period of time. The total time step is 1000, but only a section is presented for clarity.

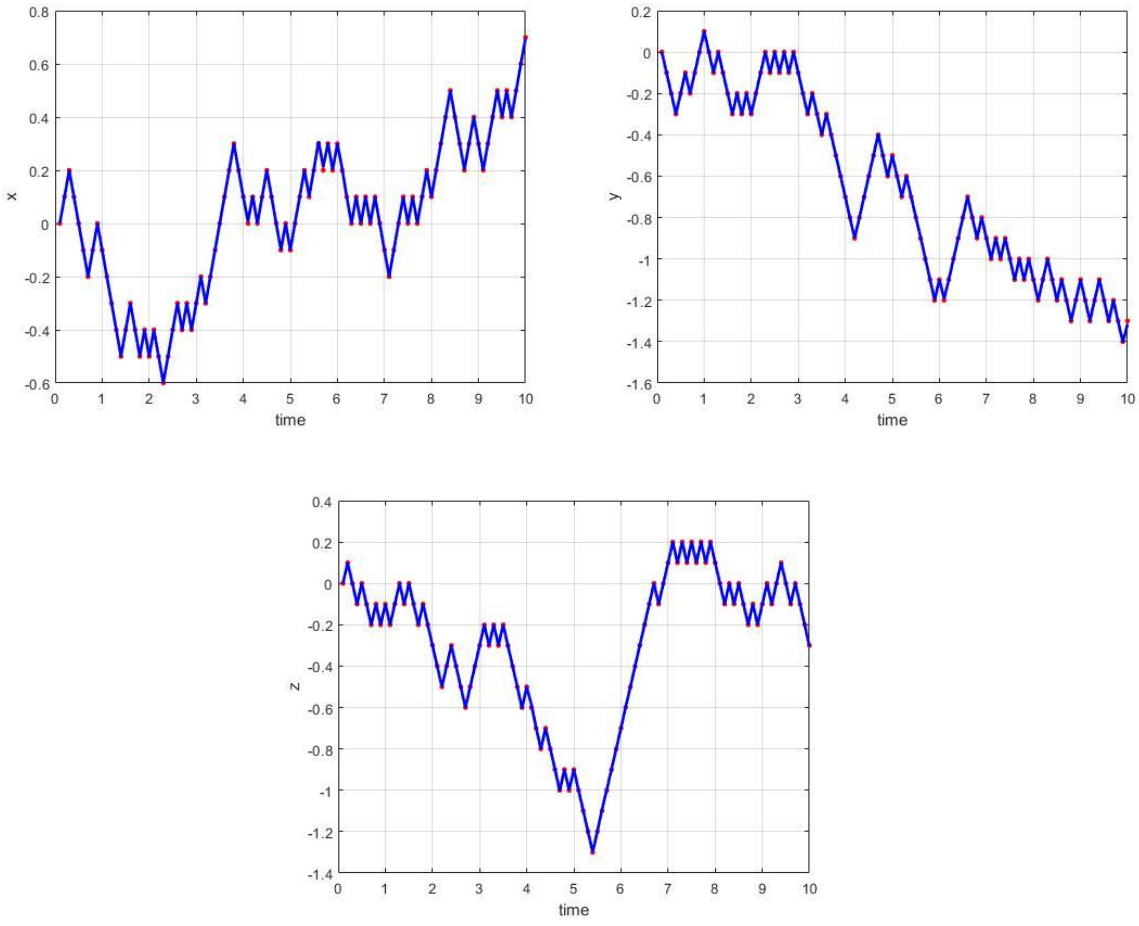

Figure 11: The x, y and z component particle reconstruction using hybrid numerical method algorithm for the case with sudden change in particle position (no noise).

Similarly, the particle orientation is simulated to vary at regular intervals of time and the position vector along all the three co-ordinates is kept constant. The normalized magnetic moment is set to be 0.01 Am^2. The reconstruction of the particle orientation against the original trajectory is displayed in *Figure 12*. It can be observed that the sudden changes in the orientation is well captured by the algorithm over a period of time. The total time step is 1000, but only a section is presented for clarity.

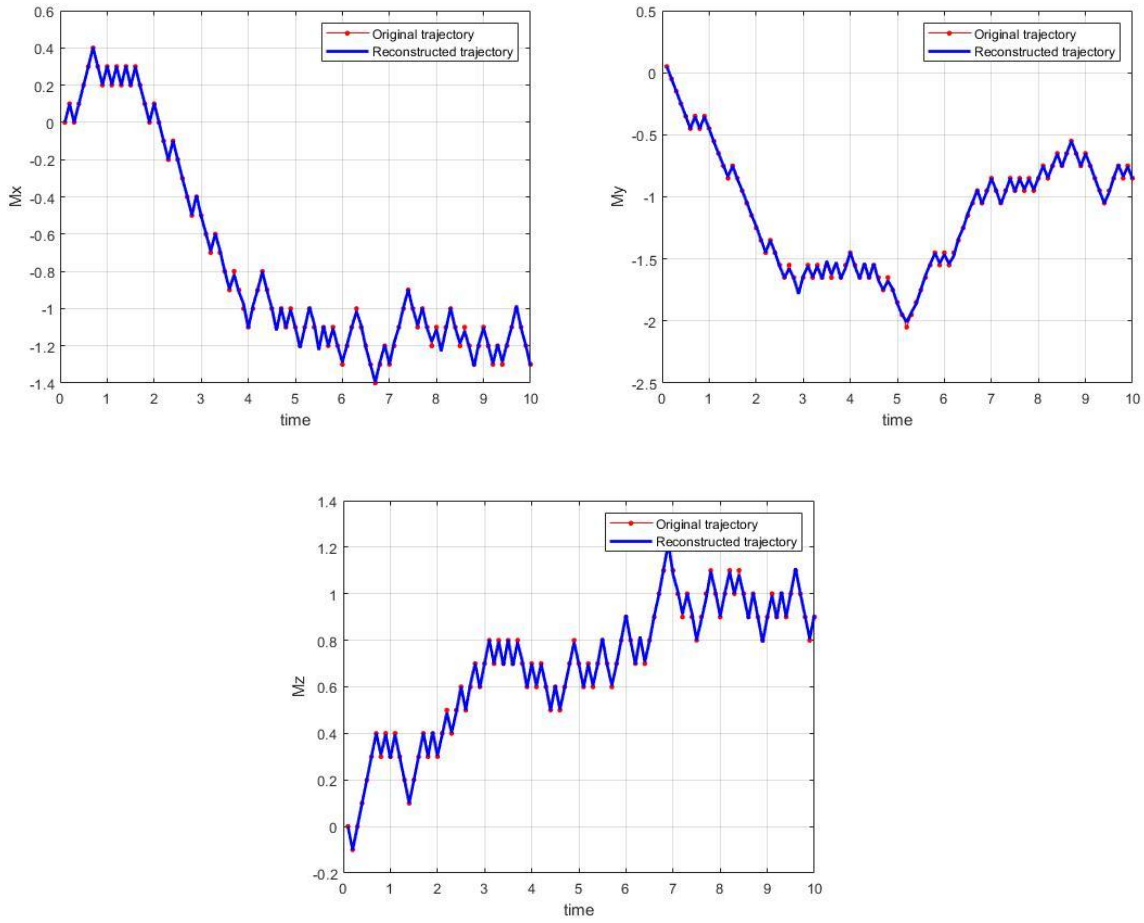

Figure 12: The M_x, M_y and M_z component particle reconstruction using hybrid numerical method algorithm for the case with sudden change in particle orientation (no noise).

The performance of the algorithm is tested by adding 3% Gaussian noise to the synthetic sensor readings. *Figure 13* shows the particle's position reconstruction with a 3% noise added to the system. It can be seen that the algorithm is able to cope with the sudden changes in the position and reconstruct the trajectory relatively well.

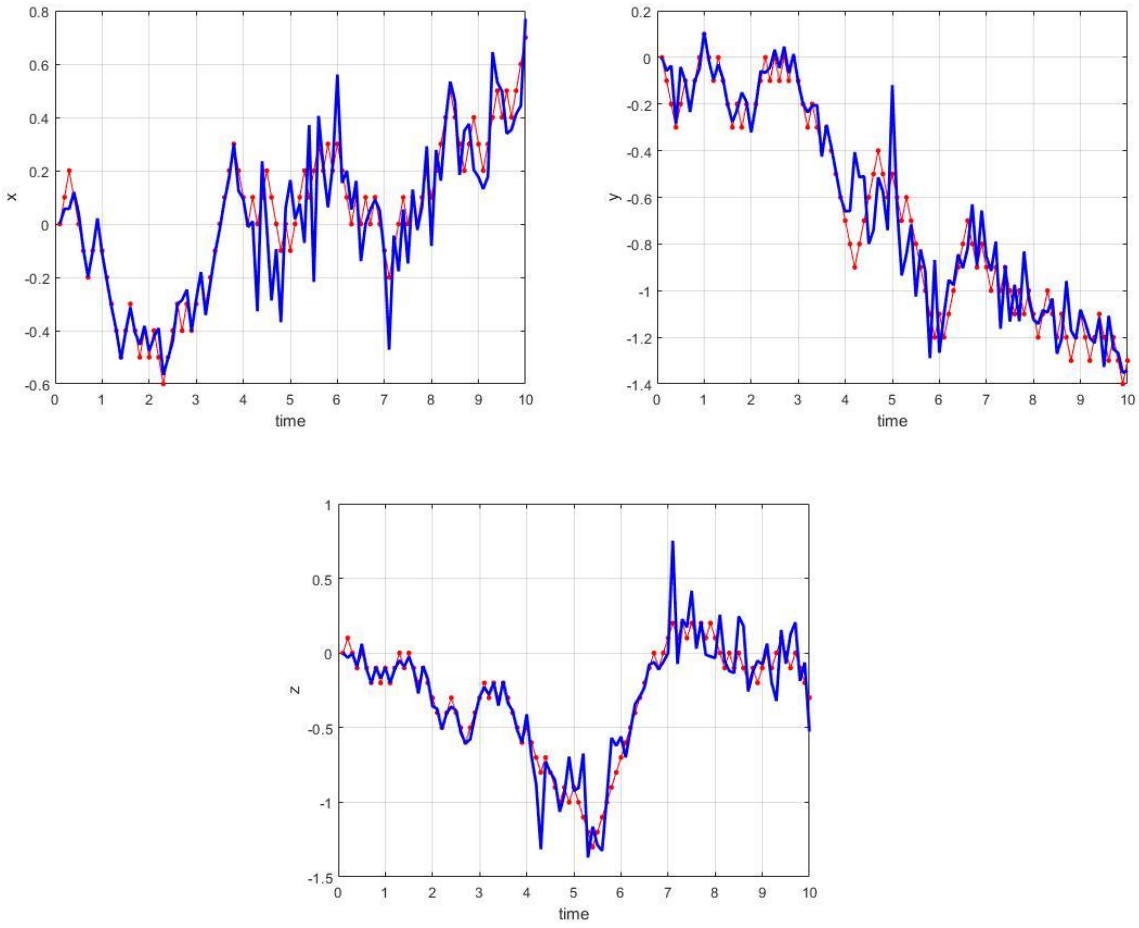

Figure 13*:* The x, y and z component particle reconstruction using hybrid numerical method algorithm for the case with sudden change in particle position (3% noise).

Figure 14 shows the particle's orientation reconstruction with a 3% noise added to the system. It can be seen that the algorithm is able to cope with the sudden changes in the position and reconstruct the trajectory relatively well.

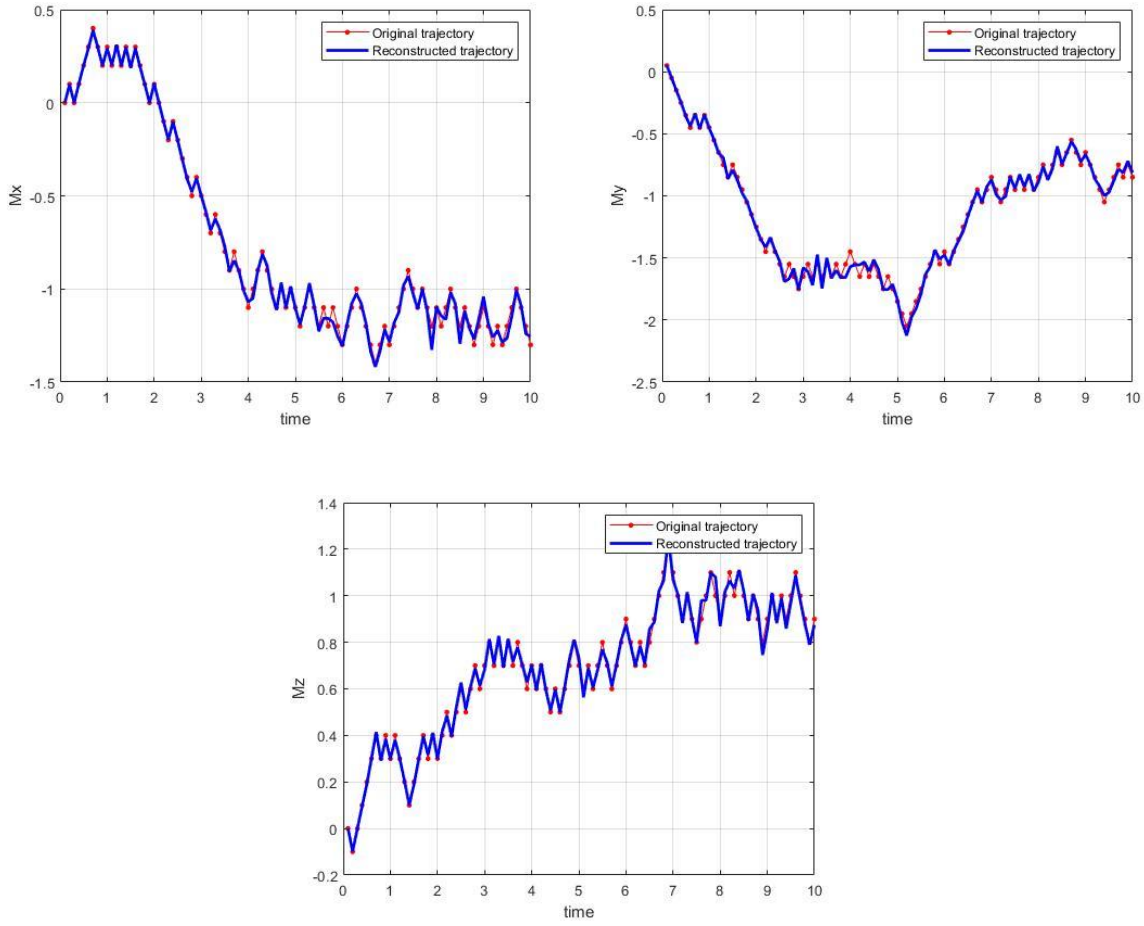

Figure 14: The M_x, M_y and M_z component particle reconstruction using hybrid numerical method algorithm for the case with sudden change in particle orientation (3% noise).

Since we were able to reconstruct the particle's position and orientation for sudden changes in the particle's position and orientation over a period of time, we should be able to reconstruct a random motion like the Brownian motion. This case has been presented in the following section.

4.5 Brownian motion

4.5.1 Introduction

Brownian motion is the random motion of particles suspended in a fluid resulting from their collision with fast moving molecules in the fluid. The fluids overall linear and angular momenta remain zero over time. Therefore, the Brownian motion should work as the perfect numerical simulation model to test the 3D Hybrid Numerical Optimization algorithm. If a particle following the Brownian motion trajectory in 3D can be reconstructed using the MPT algorithm, then basically any kind of particle trajectory can be reconstructed.

The simulation of a single particle confined in a 3D domain is shown in *Figure 15*.

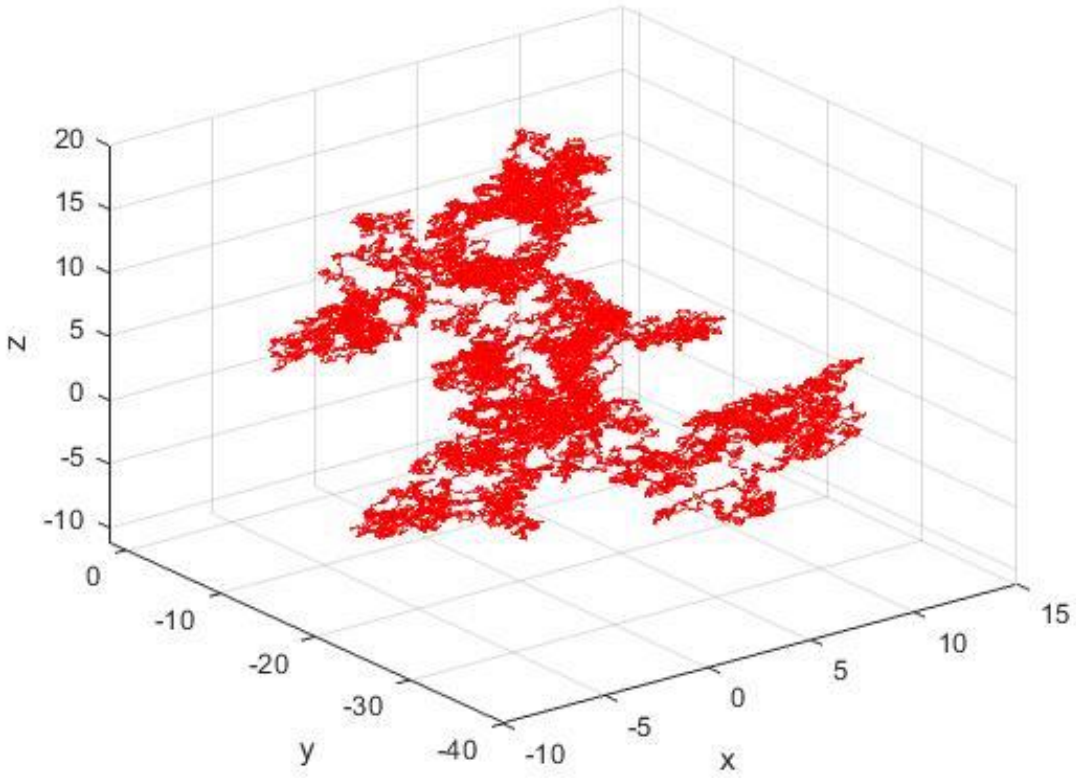

Figure 15: Trajectory of a single particle following Brownian motion in 3D

4.5.2 Results and Discussion

A single particle 3D Brownian motion trajectory is simulated using MATLAB. The particle orientation is randomised as well. The normalized magnetic moment is set to be 0.01 Am^2. The resultant synthetic sensor readings are used as input to the MPT algorithm and the reconstruction trajectory is obtained.

To evaluate the robustness of the algorithm at multiple noise levels, Gaussian noise is added to the synthetic sensor readings. Specifically, for the i^{th} sensor at each time step, O_i is set to be $B(r, r_{0i}, m).S_i\,.(1+\varepsilon)$, where ε is selected to be 0.01, 0.03, 0.06, 0.1 and 0.2 in different simulations. Multiple trajectories are reconstructed based on the data with these noise levels. The total time step in the synthetic trajectory is 5000, but only a section is presented for clarity.

Figure 16 show the reconstructed particle position along x, y and z co-ordinates respectively. It can be observed that the reconstruction results are fairly accurate. The percent error in position reconstruction using the hybrid numerical method is only 0.0075. Similarly, *Figure 17* show the reconstructed trajectory for M_x, M_y and M_z respectively. The reconstruction error in orientation using the hybrid numerical method is 0.071 degrees. This compares well with the results from SQP, SIR and EKF algorithm used for a similar simulation [30]. The comparison of the four algorithms has been presented later in this section.

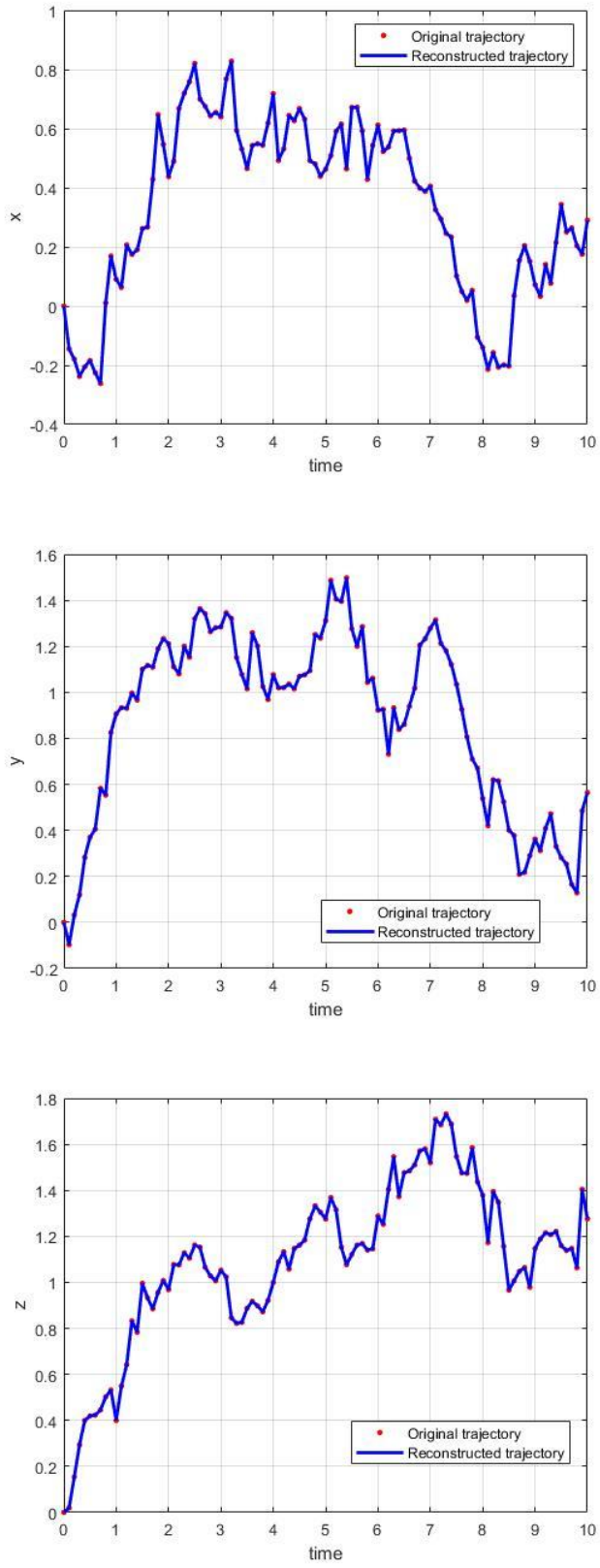

Figure 16: Sample trajectory sections reconstructed for Brownian motion using the hybrid numerical method with no noise for x, y and z component.

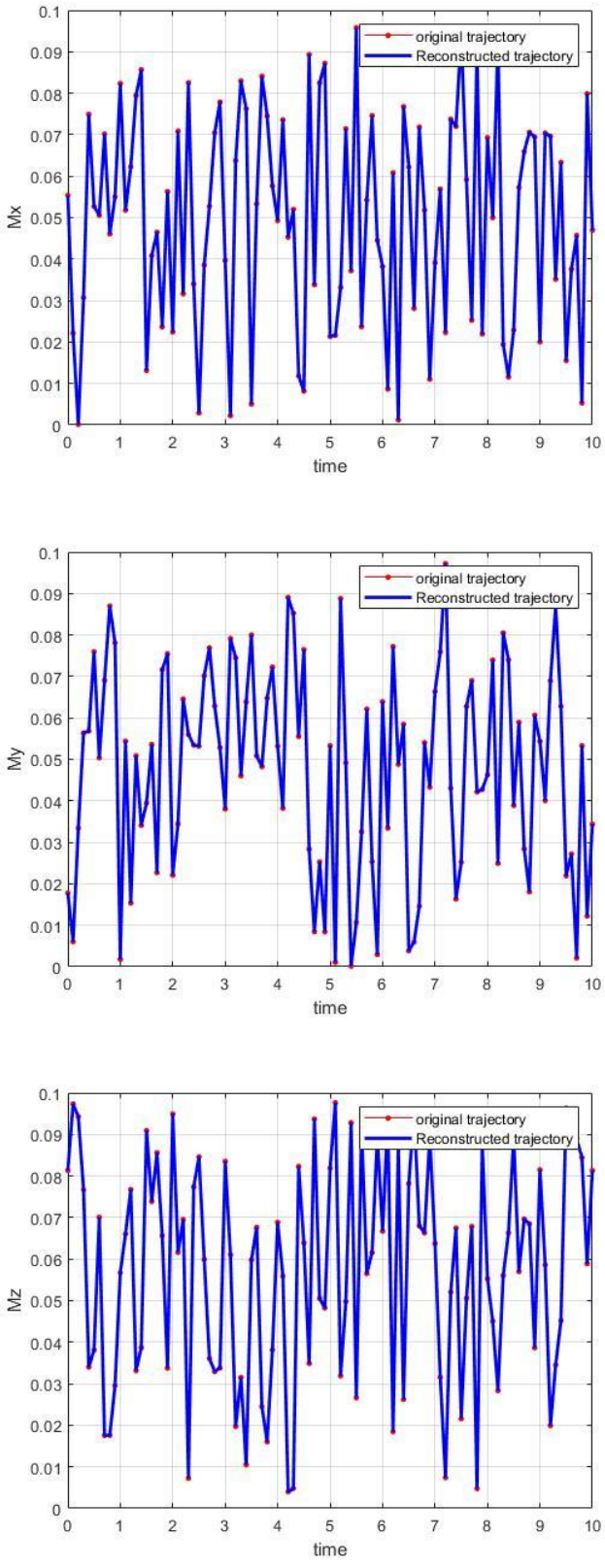

Figure 17: Sample trajectory sections reconstructed for Brownian motion using the hybrid numerical method with no noise for M_x, M_y and M_z component.

To evaluate the error in orientation, we take the inner product of the measured *m* and the reconstructed *m**. From vector properties, we know that the two vectors are well aligned if their dot product is 1. *Figure 18* shows the alignment error for the reconstruction of the Brownian motion simulation with no noise using hybrid numerical method.

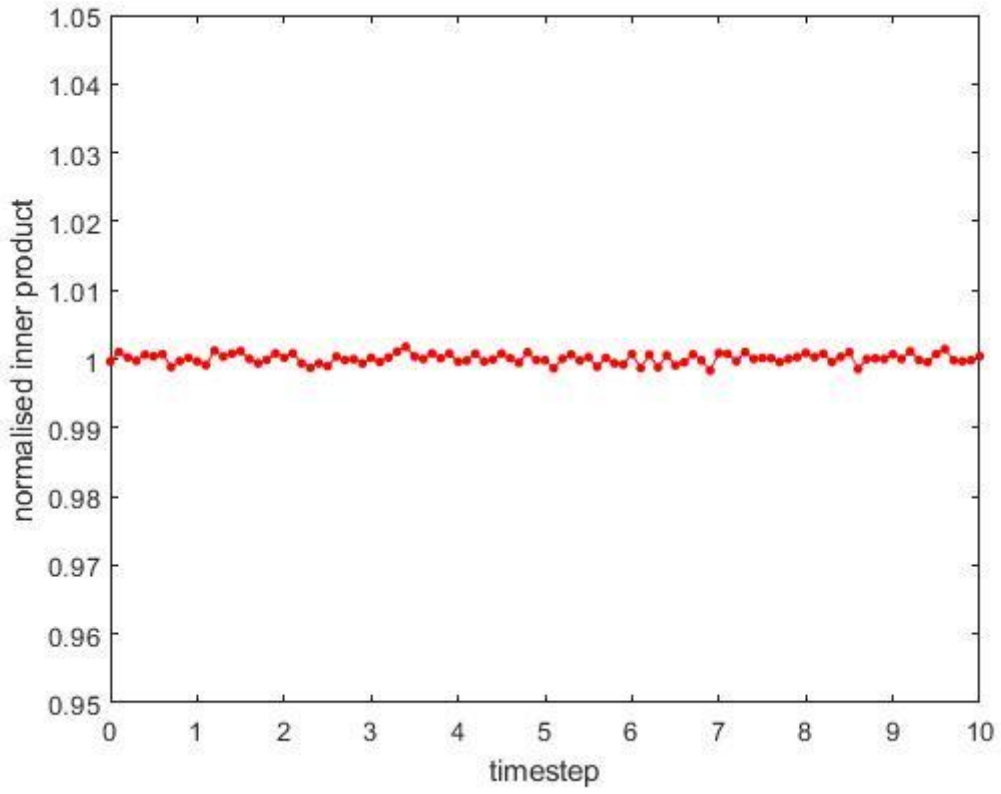

Figure 18: Normalised magnetic moment over time using hybrid numerical method with no noise

To evaluate the robustness of the algorithm, 3% Gaussian noise is added to the synthetic sensor readings. Figure 19 show the reconstructed particle position along x, y and z co-ordinates respectively and Figure 20 shows the reconstructed trajectory for M_x, M_y and M_z respectively. It can be observed that the reconstructions results adapt well to the noise in the synthetic reading keeping the results acceptable. The percentage error in position reconstruction is 0.8633 while the orientation error is 1.5 degrees.

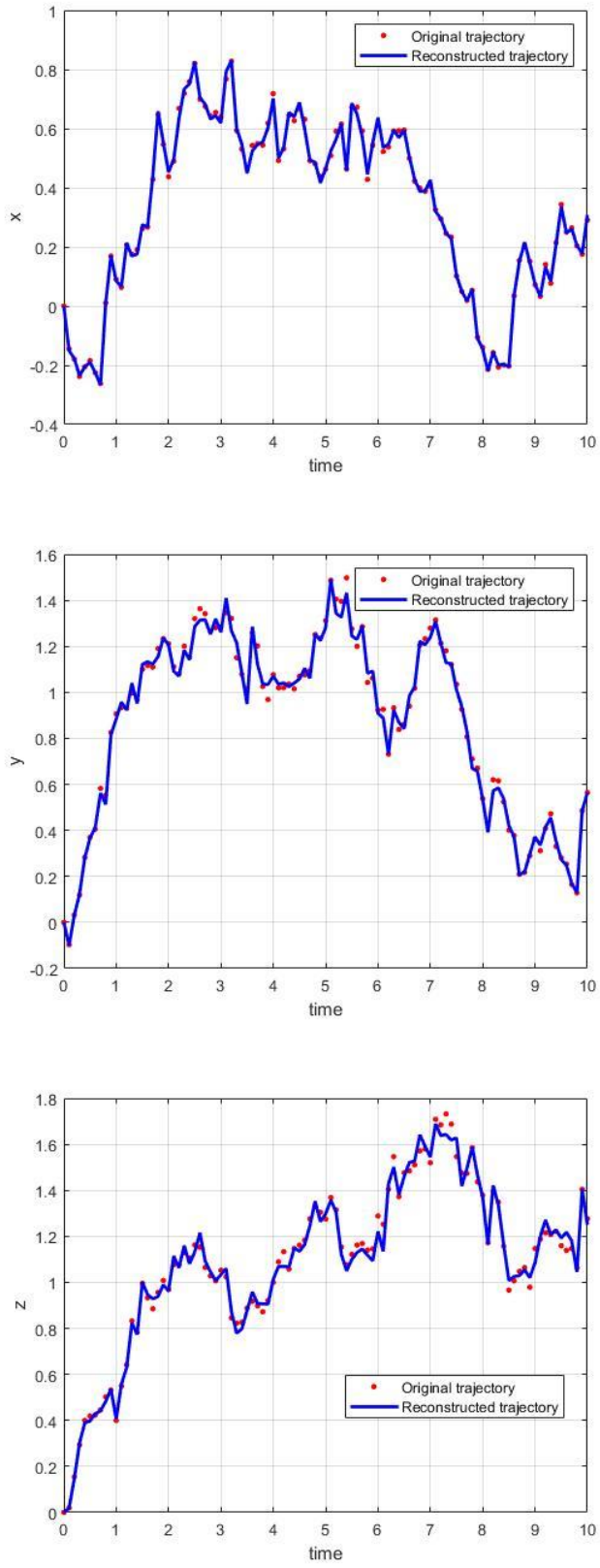

Figure 19: Sample trajectory sections reconstructed for Brownian motion using the hybrid numerical method with 3% noise for x, y and z component.

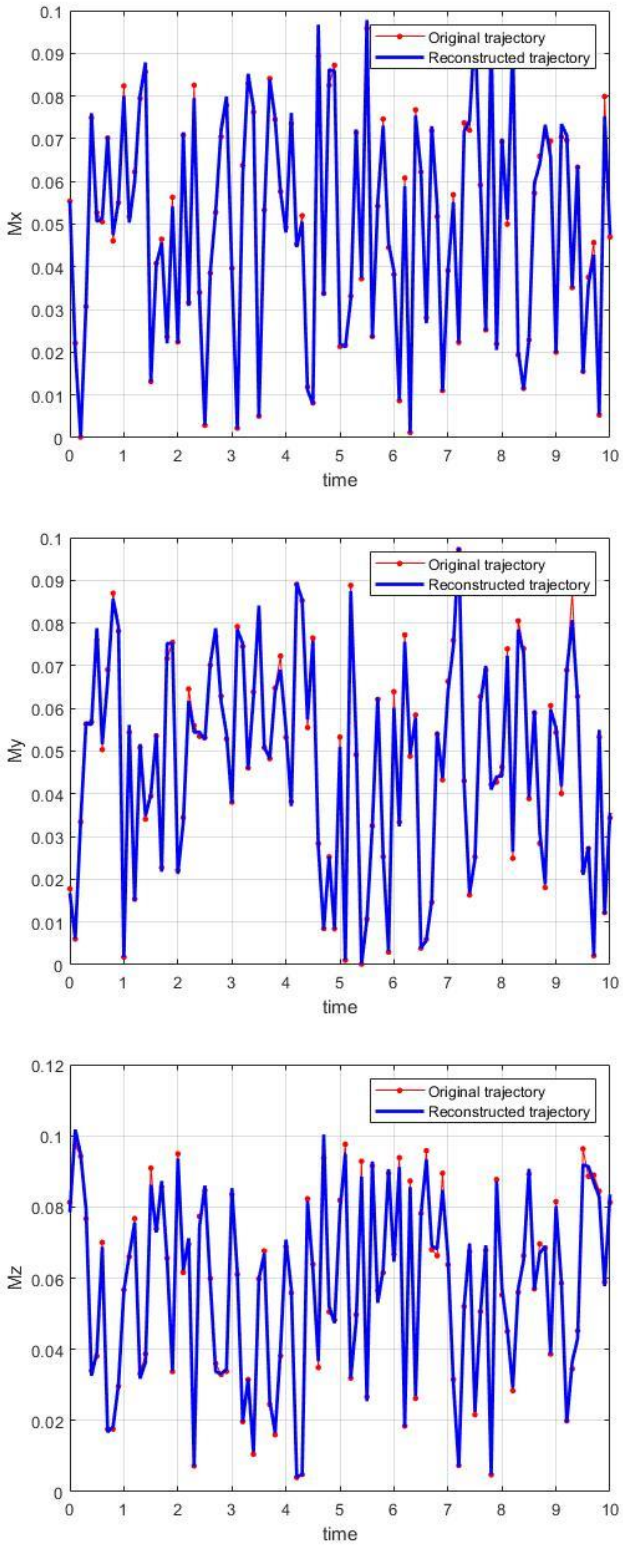

Figure 20: Sample trajectory sections reconstructed for Brownian motion using the hybrid numerical method with 3% noise for M_x, M_y and M_z component.

Further, Figure 21 and Figure 22 show the particle trajectory reconstruction and the orientation error for the Brownian motion simulation using the hybrid numerical method with 10% noise in the synthetic readings. With this amount of noise in the data, the position error is as high as 1.989 while the orientation error is 2.28 degrees.

It can be observed in Figure 22 that the MPT algorithm is not able to reconstruct the particle's orientation accurately when the noise level reaches 10%. The original orientation is completely out of phase with the reconstructed orientation over a period of time. Hence, it can be concluded that the hybrid numerical algorithm only works when the noise level in the system is limited to 6% or below. This should not be a concern since the noise level in a typical magnetometer rarely exceeds 5%. The results found for the noise level below 5% were found to be acceptable and the reconstruction accuracy was comparable with the state-of-the-art optimization algorithms available in literature.

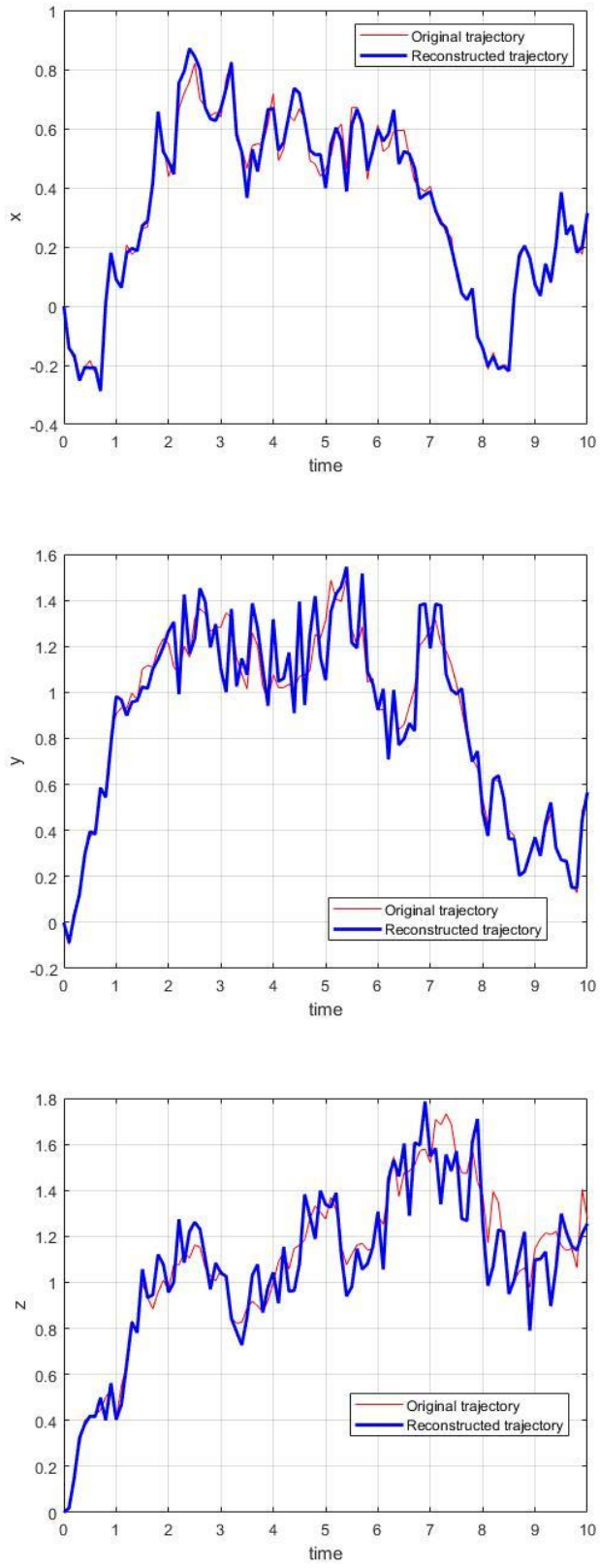

Figure 21: Sample trajectory sections reconstructed for Brownian motion using the hybrid numerical method with 10% noise for x, y and z component.

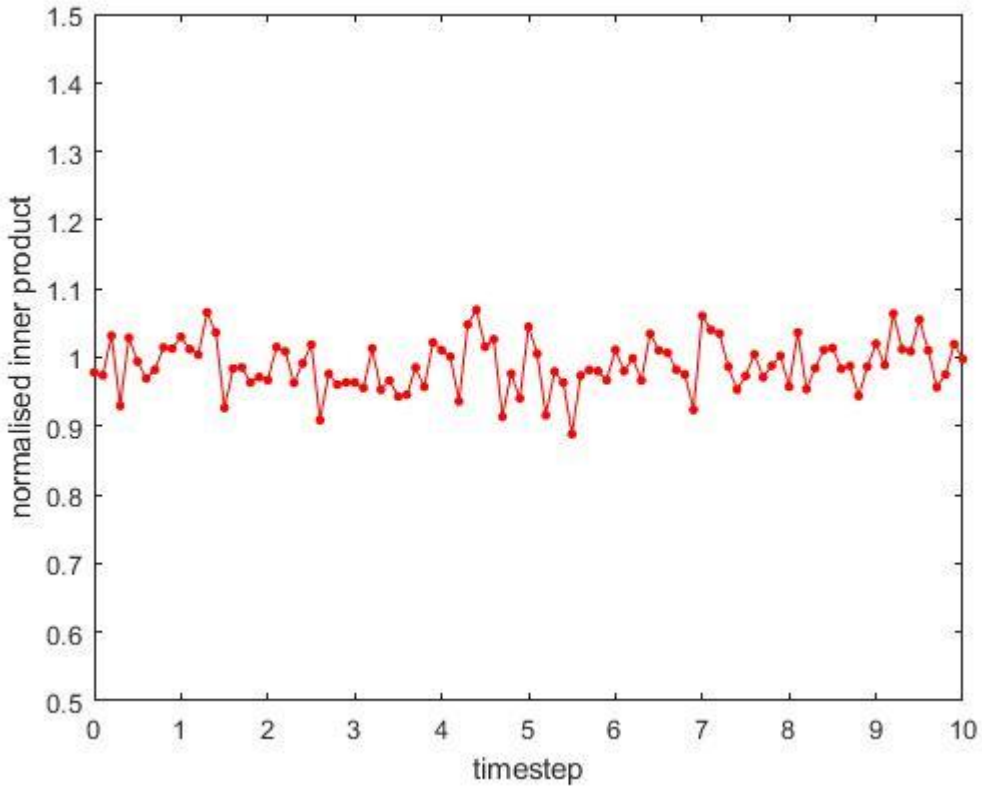

Figure 22: Normalised magnetic moment over time using hybrid numerical method with 10% noise

To set a standard in estimating the accuracy of the MPT reconstruction, we define the relative error as the difference between the real and reconstructed positions divided by the domain size. For the x component,

$$E_x = \frac{mean(|x_j^* - x_j|)}{L_x} \tag{36}$$

where, L_x is the size of the domain in the x direction;

$$L_x = \max(x) - \min(x) \tag{37}$$

x_j^* is the real value of the position and x_j is the reconstructed value. In this simulation, x_j^* is the position of the synthetic trajectory. Similarly, the values of error in the y and z component

can be calculated following Equation (36). Consequently, the average relative position error of all components is given as,

$$Position\ error = \frac{1}{3}\left(E_x + E_y + E_z\right) \tag{98}$$

Table 2 and *Figure 23* shows the uncertainties in the position obtained from the above simulation.

Table 2: The position error vs the level of noise

Error	**Method**	**No noise**	**1%**	**3%**	**6%**	**10%**	**20%**
Position error (%)	**HNM**	0.0075	0.3201	0.8633	1.3723	1.9899	5.6578
	SQP	0.003	0.21	0.6	1.1	1.49	8.41
	EKF	0.24	0.3	0.52	0.94	1.51	9.88
	SIR	0.41	0.5	0.86	1.56	-	-

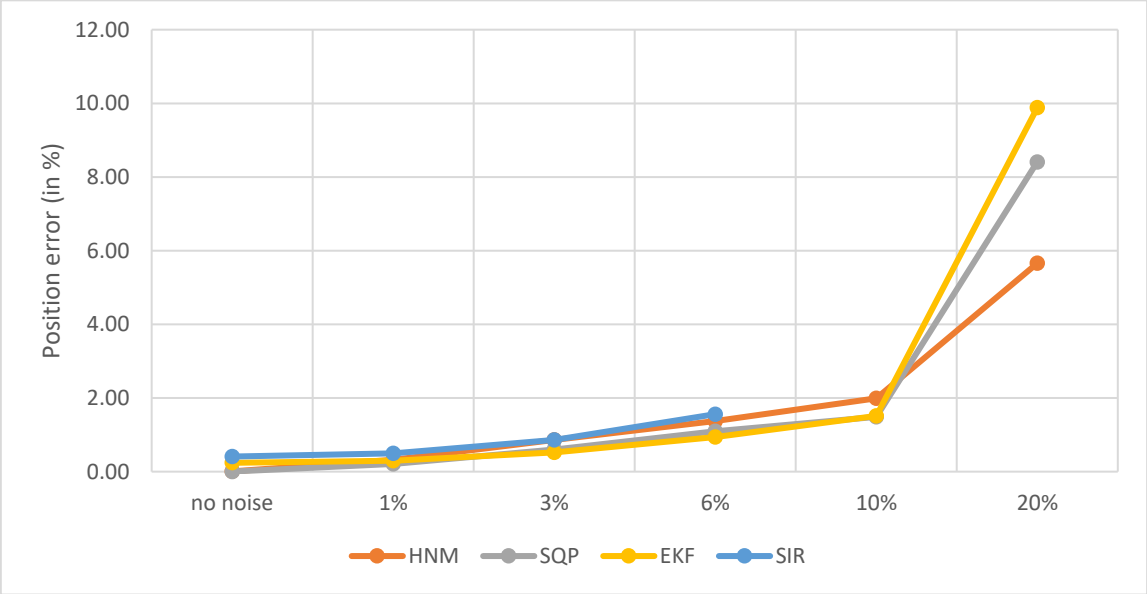

Figure 23: Position error dependence on the noise

The orientation error can be calculated by using the mean angle between the measured vector m and the real m^*. This can be done by taking the dot product of the two normalised vectors, this gives a value between -1 and 1. If the value is -1, it indicates that the two vectors are oppositely orientated, and perpendicular if the dot product is 0. If the dot product is 1, it indicates perfect alignment. Although to have a little tolerance, we will set up all the values above 0.8 to be well aligned for the above simulation. Therefore, mean of the angles with dot product below 0.8 will give us the orientation error in the reconstruction. *Table 3* and *Figure 24* shows the uncertainties in the position obtained from the above simulation.

Table 3: The rotation error vs the level of noise

Error	**Method**	**No noise**	**1%**	**3%**	**6%**	**10%**	**20%**
Rotation error (deg)	**HNM**	0.071	0.92	1.5	1.77	2.28	6.18
	SQP	0.053	0.3	0.83	1.61	2.6	5.73
	EKF	0.76	0.81	1.1	1.78	2.7	5.54
	SIR	1.43	1.43	1.74	2.77	-	-

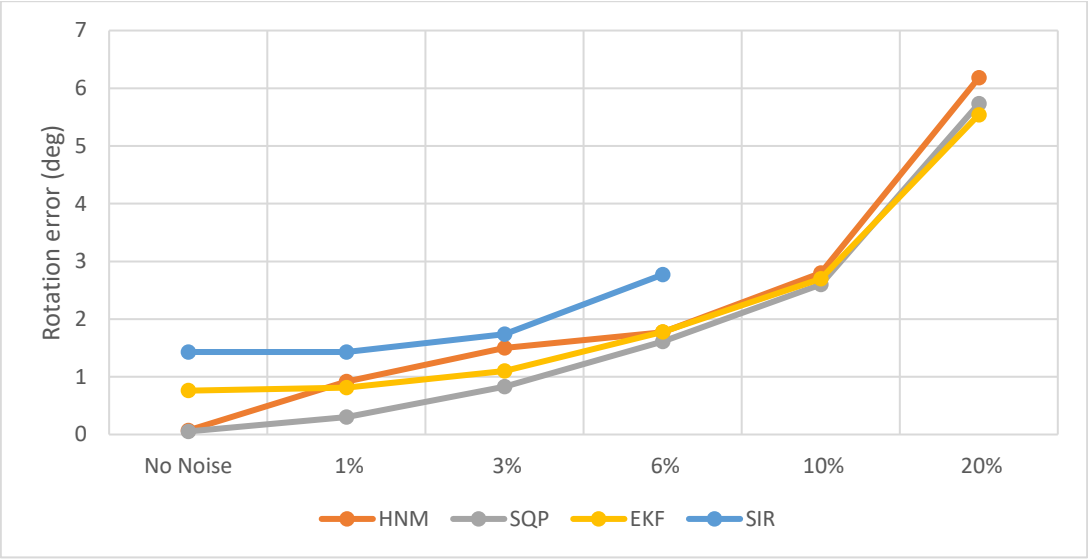

Figure 24: The rotation error vs the noise level

The reconstruction using the HNM algorithm is comparable in accuracy with the EKF, SQP and the SIR algorithms. When compared for the 3% noise case, the SQP algorithm is the most accurate. However, the computation time is huge using this algorithm. The HNM and EKF algorithm are about 10^4 orders of magnitude faster than the SQP algorithm while the SIR method takes about one-third of the time taken by the SQP algorithm. The EKF algorithm, however, requires a lot of parameters to be taken care of during data collection. HNM algorithm, on the other hand, requires only the sensor locations and the sensor readings to reconstruct the particle's position. Therefore, although, the EKF algorithm is the most effective optimization technique, for preliminary investigation, the HNM algorithm can be considered as a more viable technique.

5. Granular flow

5.1 Introduction

Granular mixing has been a part of human life since our earliest ancestors put pestle to mortar. In recent years, granular mixing has gained importance, particularly in highly-regulated industries of food and pharmaceuticals. The study of granular flow is therefore crucial when it comes to quality control of items from breakfast cereal to medicine tablets. Other industries where granular mixing plays an important role include construction (blending of building material), cosmetics (manufacture of makeup products), and household hygiene items (laundry detergents and drain decloggers) [49]. In most cases the focus is on ensuring the homogeneity of the manufactured product. Since major causes of incomplete or inefficient mixing include inefficient mixer design and segregation during mixing process, particle path lines and velocity profiles in the mixer vessel also need to be scrutinized.

Dense fluid-particle flows in which the direct particle-particle interactions are a dominant feature encompass a diverse range of industrial and geophysical contexts (Jaeger *et al.* 1996 [41]) including, for example, slurry pipelines (Shook and Roco 1991 [42]), fluidized beds (Davidson and Harrison 1971 [43]), mining and milling operations, ploughing (Weighardt 1975 [44]), abrasive water jet machining, food processing, debris flows (Iverson 1997 [45]), avalanches (Hutter 1993 [46]), landslides, sediment transport and earthquake-induced soil liquefaction. In many of these applications, stress is transmitted both by shear stresses in the fluid and by momentum exchange during direct particle-particle interactions.

When the particle-particle interaction dominates the mechanics, the motions are called granular flows and the flow patterns can be quite different from those of conventional fluids. Within the domain of granular flows, there are, as we shall see, several very different types of flow distinguished by the fraction of time for which particles are in contact. For most slow

flows, the particles are in contact most of the time. Then large transient structures or assemblages of particles known as force chains dominate the rheology and the inertial effects of the random motions of individual particles play little role. Force chains are ephemeral, quasi-linear sequences of particles with large normal forces at their contact points. They momentarily carry much of the stress until they buckle or are superseded by other chains. Force chains were first observed experimentally by Drescher and De Josselin de Jong (1972) [47] and, in computer simulations, by Cundall and Strack (1979) [48]. Their dynamics have distinctive properties from homogeneous fluids. A notable feature is their tendency to concentrate shear in narrow bands at particularly low speed. The shear band has distinctive properties. For example, the shear zone at the interface between two materials is refracted in analogy with the refraction of a light beam in optics; and surprisingly, the constitutive relation outside the band may depend on the motion in the band (which can be modelled using global or secondary rheology). Understanding dense granular flow remains a major challenge. It is not clear how these microscopic properties and dynamics influence the behaviour on a large scale, and a comprehensive model is needed to describe macroscopic flow based on the dynamics of a single particle.

Much effort has been devoted to studying the motion of individual particles. In the low-speed regime, the particle density is high and the enduring contact usually dominates the momentum transfer. Many experiments and simulations are performed in split-bottom geometries, e.g., the split-bottom Couette cell, where the shear band is located near the split. Thanks to the development of high-speed videoing and magnetic resonant imaging (MRI), the translational motion of a particle in both surface and bulk flows is experimentally accessible.

Recently, many researchers have paid attention to the dynamics of non-spherical particles, since the particle shape affects the macroscopic dynamics and most of the particles in nature and industry are non-spherical. Both experimental and simulation results show that the

elongated particles align with the streamline direction in the shear zone. The orientation distribution is related to the aspect ratio, and is independent of the shear rate. Particles with an aspect ratio of 1 have no significant alignment. The orientation of elongated particles can be modelled following the director dynamics in a nematic liquid crystal (the Leslie-Ericksen equations); however, the underlying physics is drastically different, as in the liquid crystal case, thermal fluctuation plays a key role.

Since a magnetic field can easily penetrate non-magnetic materials, the MPT technique can be used in an opaque environment like granular flows. Therefore, we use the MPT technique described in chapter 3 using the Hybrid Numerical Optimization method to study the granular flow. The experimental setup and the results are discussed below.

5.2 Experimental setup

The experiment is conducted in an environment without any ferromagnetic material. The whole device is placed in a Helmholtz coil that balances the Earth magnetic field. The orientation has to be set opposite to the earth's magnetic field and current through the coil has to be set such that the strength of the field equals the earth's magnetic field, following the Biot-Savart's law. The two fields will oppose each other, cancelling each other out. This will allow the tracer particle to orientate freely. To generate a granular shear flow, we use a cylindrical container with a rotating disc at the bottom as shown in Figure 25. The rotating disc is connected by a shaft to a DC motor that is located 65 centimetres away from the measurement domain to ensure that the motor has little effect in the measurement domain. This distance is sufficient to prevent the motor magnetic field from interfering with the MPT measurements. The inner diameter of the cylindrical container is, D_c = 101 mm, and the rotating disc diameter is, D_r = 63.5 mm (D_c /D_r = 0.63). To ensure the bottom disk provides consistent shear rate, one layer of granular material is glued on it.

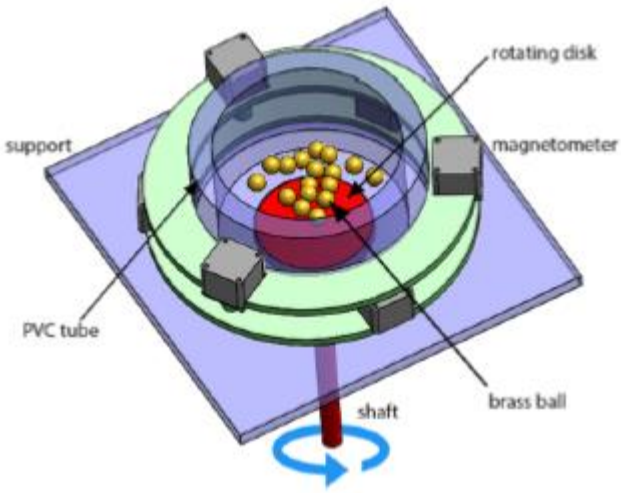

Figure 25: An illustration of the device used to generate a granular shear flow (the Helmholtz coil is not shown here) [29]

Several spherical plastic balls of diameter 25 mm are randomly packed in the container. The filling height H = 50 mm. A cylindrical sample particle is used to study the dynamics of non-spherical particles in the flow. The cylinder diameter is also 25 mm and its aspect ratio is 1. A small neodymium magnet is inserted into the core to label this cylinder as shown in *Figure 26*. The trajectory of this sample particle can be reconstructed using the magnet field and our MPT algorithm, as described in the previous sections. The measurement takes more than 1.5 hours, and 300,000 data points are recorded.

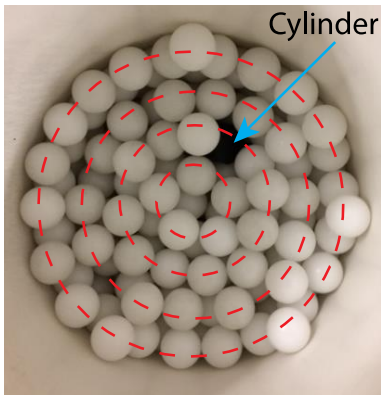

Figure 26: The top view of the plastic balls in the cylindrical container. The tracer cylindrical particle is hidden among these balls. [29]

The tracer cylindrical particle has nearly the same mechanical property as the normal balls. The rotation speed of the bottom disc is 10 rpm. The magnetometers used are Bartington M612 probes (3-axies) and are installed on two circular decks with an angular separation of 120 degrees. The distance between the decks is 37.5 mm. The magnetometers are located 67.5 mm away from the centre of the cylinder. In the measurements, the sampling frequency is set to 50 Hz, which is sufficient to catch the motion of the tracer particle, since the driving motion is slow. Table *4* summarizes the settings and the parameters of the experiment.

Table 4: Settings and Parameters of the Experimental Setup

Granular Bed	
Diameter	101 mm
Height	50 mm
Rotation speed	10 rpm
MPT Sensor Array	
Sensor type	Barington M612
Amount	4
Frequency	50 Hz
Particles	
Bed material diameter	25 mm
Bed Particle material	Plastic
Density	7.47 g.
Tracer Particle material	Plastic
Tracer Particle diameter	Cylinder with diameter 25 mm (AR 1)
Density	7.365 g.
Magnetic moment	0.0105 Am^2

5.3 Results and discussion

Since the grain diameter is large and the driving rotation is only 10 rpm, the balls show a layered distribution. The cylindrical tracer particle, which was initially near the centre, is able to reach three layers in the radial direction, as shown in Figure *27*, and four layers in the vertical direction, as shown in Figure *28*.

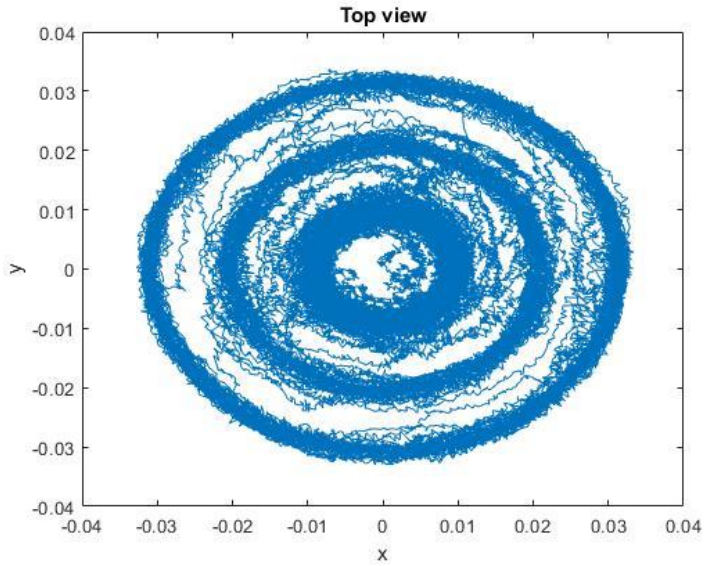

Figure 27: The top view of the trajectory of a tracer particle in a granular shear flow. The unit is meter.

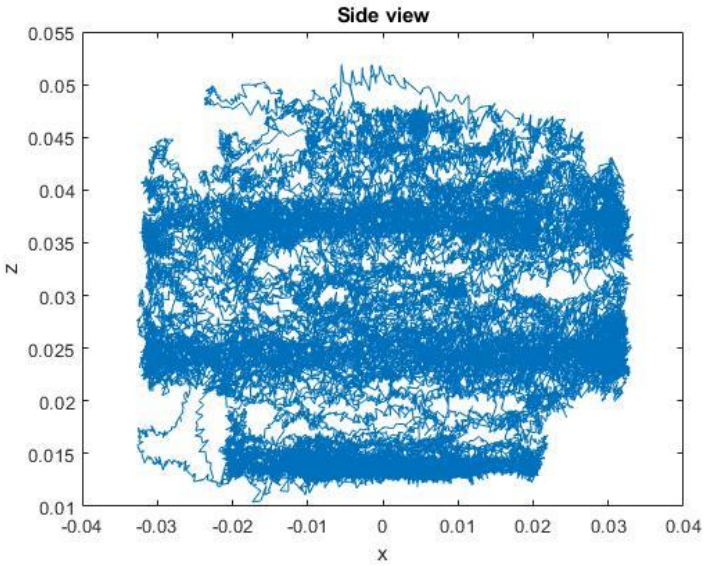

Figure 28: The side view of the trajectory of a tracer particle in a granular shear flow. The unit is meter.

The probability of staying in each layer is not the same. The radial and azimuthal probability distribution was calculated. The tracer particle has a higher probability of staying at the periphery than at the centre as seen in Figure *29.*

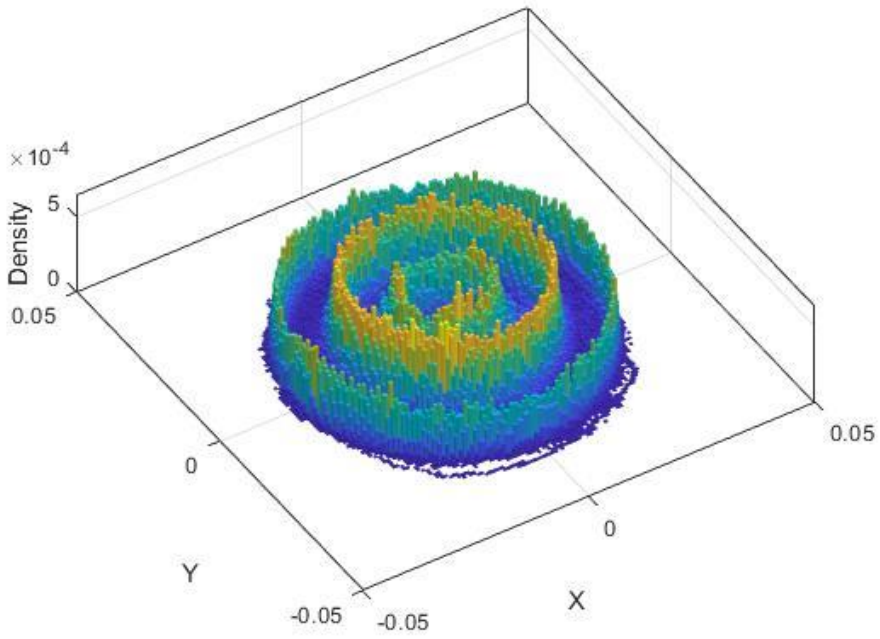

Figure 29: The probability distribution in the XY plane

When viewed from the surface, we can see that as shown in *Figure 30* that the balls travel in a layered structure. Figure *29* shows that the X-Y position distribution of the sample particle (the histogram of finding the tracer particle at given x, y location) indicates that the bulk flow also possesses the layered structure. This periphery diameter is about 70 mm, and there are two more layers of balls between this periphery and the cylinder wall. In our measurement, the cylinder has rarely reached the outer layer.

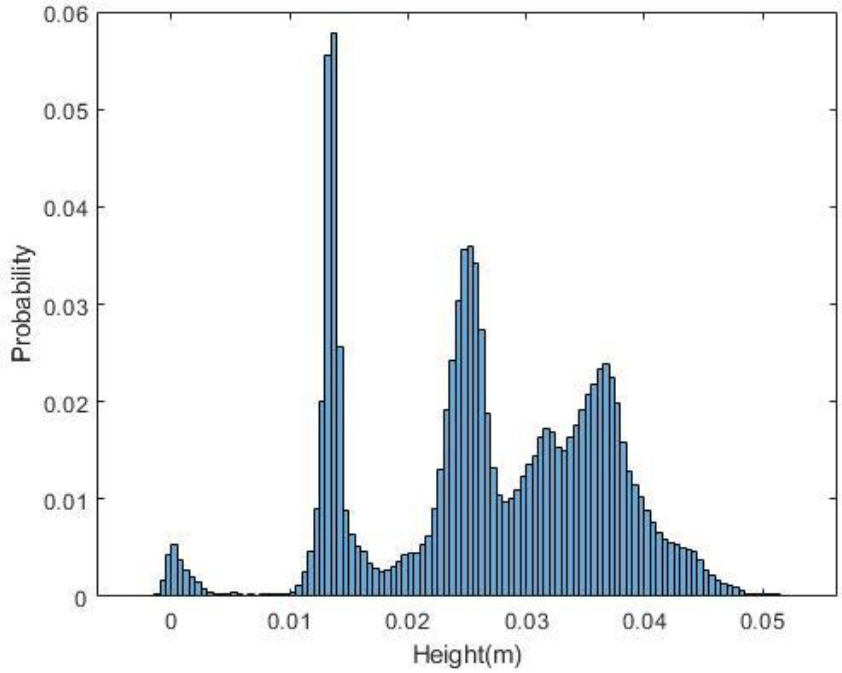

Figure 30: The probability distribution in the vertical direction

5.4 Chapter Summary

In this chapter, the MPT method based on the Hybrid Numerical Optimization Algorithm proposed in this work was used to study the dense granular shear flow in an experimental setup. The algorithm was accurately able to track the cylindrical tracer particle's position and orientation in the flow over a period of time. The probability of the particle staying in a particular layer in both the vertical and the radial direction was studied. It was observed that the tracer particle has a higher probability of staying at the periphery than at the centre. It was also observed that the tracer particle travels in a layered structure and the particle rarely reaches the outer layer. This proves that the MPT technique can be successfully used as a tool in the study of granular flow. This technique can be used to study more complex properties of granular flow like the particle-particle interaction and the tracer particle orientation in the flow for different aspect ratios and different tracer particle geometries.

6. Conclusion

In this work, a hybrid numerical algorithm to reconstruct a single particle trajectory using Magnetic Particle Tracking technique has been presented. A great advantage of the MPT method is that it does not rely on any hazardous radiation such as the X-rays to measure the motion in an opaque environment. This technique also helps us measure the position and orientation of the particle simultaneously.

The algorithm was initially validated using numerical simulations and was compared with the SQP, SIR and EKF algorithms. The accuracy of the algorithm was found to be comparable to that of the state-of-the-art optimization approach. The reconstruction speed using the hybrid numerical algorithm is orders of magnitude faster. The EKF and the HNM algorithm are about 10^4 orders of magnitude faster than the SQP algorithm while the SIR algorithm take about one-third of the time as the SQP algorithm. The HNM when compared with the EKF algorithm, is much simpler to use as it does not have a lot of parameters to take care of. The numerical simulation for the Brownian motion showed that the MPT position uncertainty can reach 0.86 % and the angular error is 1.5^o for a measurement domain with a size of about 10 cm. The algorithm performance with Gaussian noise added to the synthetic sensor reading was also observed to be satisfactory for noise levels below 6%.

The MPT technique was later used to track the motion of a tracer particle in a dense granular shear flow. The results demonstrate that the MPT is able to capture the trajectory of a cylindrical particle, from which it is able to obtain the spatial probability distribution in both the radial and the vertical directions. The trajectory of the tracer particle demonstrated that the bulk flow possesses a layered structure. Because of the stated advantages and its high accuracy, MPT is a powerful tool for studying dense granular flows.

7. Recommendations

For future works, the following improvements could be made and tested:

- Tracer particle with different geometries can be tested in the above described experimental setup. Complex particle-particle interaction properties like the preferred orientation of the tracer particle with respect to the bulk material can be analysed for different tracer particle geometries and aspect ratios.
- The trajectory of multiple particles can be reconstructed. This would introduce complications as multiple magnetic particles in a confined setup would mean that the tracer particle could interact with one another and could stick together and become one particle during the experiment. This would prevent performing experiments for a longer duration. The setup would also require a greater number of sensors. But this is certainly something to be considered for the future.
- New and better optimization algorithm can be tested and compared with the algorithms presented in this work.

8. References

[1] Ludwig Prandtl [https://en.wikipedia.org/wiki/Ludwig_Prandtl]

[2] "Review of non-invasive methods to characterize granular mixing", Humair Nadeem, Therodore J. Heindel. Powder Technology, Elsevier (2017).

[3] "Optical visualization and composition analysis to quantify continuous granular mixing processes", T.A. Kingston, T.J. Heindel, Powder Technol. 262 (2014).

[4] "Experiments and simulations of cohesionless particles with varying roughness in a bladed mixer ",B. Remy, T.M. Canty, J.G. Khinast, B.J. Glasser, Chem. Eng. Sci. (2010).

[5] "Granular flow and segregation in a four-bladed mixer", S.L. Conway, A. Lekhal, J.G. Khinast, B.J. Glasser, Chem. Eng. Sci. 60 (2005).

[6] "Characterization of granular flow of wet solids in a bladed mixer",A. Lekhal, S.L. Conway, B.J. Glasser, J.G. Khinast, AICHE J. 52 (2006).

[7] "Polydisperse granular flows in a bladed mixer: experiments and simulations of cohesionless spheres", B. Remy, J.G. Khinast, B.J. Glasser, Chem. Eng. Sci. 66 (2011).

[8] "Wet granular flows in a bladed mixer: experiments and simulations of monodisperse spheres", B. Remy, J.G. Khinast, B.J. Glasser, AICHE J. 58 (2012).

[9] "Non-invasive tomographic and velocimetric monitoring of multiphase flows", J. Chaouki, F. Larachi, M.P. Duduković, Ind. Eng. Chem. Res. 36 (1997).

[10] "Optimal design of radioactive particle tracking experiments for flow mapping in opaque multiphase reactors ", S. Roy, F. Larachi, M.H. Al-Dahhan, M.P. Duduković, Appl. Radiat. Isot. 56 (2002).

[11] “Investigating the dynamics of cylindrical particles in a rotating drum using multiple radioactive particle tracking”, M. Rasouli, O. Dubé, F. Bertrand, J. Chaouki, AICHE J. 62 (2016).

[12] “Positron emission particle tracking studies of spherical particle motion in rotating drums”, D.J. Parker, A.E. Dijkstra, T.W. Martin, J.P.K. Seville, Chem. Eng. Sci. 52 (1997).

[13] “Investigation of the effect of impeller rotation rate, powder flow rate, and cohesion on powder flow behavior in a continuous blender using PEPT”, P.M. Portillo, A.U. Vanarase, A. Ingram, J.K. Seville,M.G. Ierapetritou, F.J. Muzzio, Chem. Eng. Sci. 65 (2010).

[14] “Positron imaging systems for studying particulate, granular and multiphase flows”, T.W. Leadbeater, D.J. Parker, J. Gargiuli, Particuology 10 (2012).

[15] “High-resolution monitoring of the gastrointestinal transit of a magnetically marked capsule “, Weitschies W, K¨otitz R, Cordini D and Trahms L, *J. Pharm. Sci.*(1997).

[16] “A novel method for real-time magnetic marker monitoring in the gastrointestinal tract”, Wilfried Andrä *et al*, *Phys. Med. Biol* (2000).

[17] G. Mohs, O. Gryczka, and S. Heinrich, Chem. Eng. Sci. **64**, 4811 (2009).

[18] V. Idakiev and L. Mörl, J. Chem. Technol. Metall. **48**, 445 (2013).

[19] E. E. Patterson, J. Halow, and S. Daw, Ind. Eng. Chem. Res. **49**, 5037 (2010).

[20] A. Köhler, D. Pallarès, and F. Johnsson, Fuel Process. Technol. **162**, 147 (2017).

[21] A. Köhler, A. Rasch, D. Pallarès, and F. Johnsson, Powder Technol. **316**, 492 (2017).

[22] L. Zhang, F. Weigler, V. Idakiev, Z. Jiang, L. Mörl, J. Mellmann, and E. Tsotsas, Powder Technol. **339**, 817 (2018).

[23] F. Charru, B. Andreotti, and P. Claudin, Annu. Rev. Fluid Mech. **45**, 469 (2013).

[24] F. Toschi and E. Bodenschatz, Annu. Rev. Fluid Mech. **41**, 375 (2009).

[25] N. Chenouard, I. Smal, F. De Chaumont, M. Maška, I. F. Sbalzarini, Y. Gong, J. Cardinale, C. Carthel, S. Coraluppi, M. Winter, A. R. Cohen, W. J. Godinez, K. Rohr, Y. Kalaidzidis, L. Liang, J. Duncan, H. Shen, Y. Xu, K. E. G. Magnusson, J. Jaldén, H. M. Blau, P. Paul-Gilloteaux, P. Roudot, C. Kervrann, F. Waharte, J. Y. Tinevez, S. L. Shorte, J. Willemse, K. Celler, G. P. Van Wezel, H. W. Dan, Y. S. Tsai, C. O. De Solórzano, J. C. Olivo-Marin, and E. Meijering, Nat. Methods **11**, 281 (2014).

[26] A. Amon, P. Born, K. E. Daniels, J. A. Dijksman, K. Huang, D. Parker, M. Schröter, R. Stannarius, and A. Wierschem, Rev. Sci. Instrum. **88**, 051701 (2017).

[27] J. S. Lin, M. M. Chen, and B. T. Chao, AIChE J. **31**, 465 (1985).

[28] D. Parker, D. Allen, D. Benton, P. Fowles, P. McNeil, M. Tan, and T. Beynon, Nucl. Instrum. Methods Phys. Res., Sect. A **392**, 421 (1997).

[29] "A comparison of Sequential Quadratic Programming Algorithm and Extended Kalman Filter Method in the Magnetic Particle Tracking Reconstruction", Xingtian Tao, Huixuan Wu, AIAA (2019).

[30] "A new development in magnetic particle tracking technology and its application in a sheared dense granular flow", Xingtian Tao, Xuemin Tu, Huixuan Wu, Review of Scientific Instruments (2019).

[31] C. Hu, M. Li, S. Song, W. Yang, R. Zhang, and M. Q. Meng, IEEE Sens. J. **10**, 903 (2010).

[32] " Magnetic Particle Tracking for nonspherical particles in a cylindrical fluidized bed", Kay A. Buist, P. Jayaprakash, J.A.M. Kuipers, AlChE (2017).

[33] "Determination and comparison of rotational velocity in a pseudo 2D fluidized bed using magnetic particle tracking and discrete particle modelling", K.A. Buist, T.W. van Erdewijk, N.G. Deen and J.A.M. Kuipers, AlChE (2105).

[34] "Improved Magnetic Particle Tracking Technique in Dense Gas Fluidized Beds", Kay A. Buist, Alex C. van der Gaag, Niels G. Deen, and Johannes A. M. Kuipers, AlChE (2014).

[35] Y. Shi and H. Fang, Int. J. Control **83**, 538 (2010).

[36] F. Gustafsson, Adaptive Filtering and Change Detection (Wiley, New York,2000).

[37] M. S. Arulampalam, S. Maskell, N. Gordon, and T. Clapp, IEEE Trans. Signal Process. **50**, 174 (2002).

[38] A. Smith, Sequential Monte Carlo Methods in Practice (Springer Science & Business Media, 2013).

[39] R. E. Kalman and R. S. Bucy, J. Basic Eng. **83**, 95 (1961).

[40] A. J. Chorin and X. Tu, Proc. Natl. Acad. Sci. U. S. A. **106**, 17249 (2009).

[41] "Granular solids, liquids, and gases", Heinrich M. Jaeger and Sidney R. Nagel.

[42] "Slurry Flow: Principles and Practice", Book by C. A. Shook and Mihail Roco.

[43] "Fluidization", David Harrison, JSTOR (1971).

[44] "Experiments in Granular Flow", R. Weighardt, Annual Review of Fluid Mechanics (1975).

[45] "The physics of debris flows", Richard M. Iverson, Review of Geophysics (1997).

[46] "Continuum Mechanics in Environmental Sciences and Geophysics", Hutter K., Springer (1993)

[47] "Photo elastic verification of a mechanical model for the flow of a granular material", A.Drescher, G.de Josselin de Jong, Journal of Mechanics and Physics of Solids, Elsevier (1972).

[48] “A discrete numerical model for granular assemblies”, P.A Cundall, O.D.L. Strack, Geotechnique (1979).

[49] “Powder mixing: Some practical rules applied to agitated systems”, M. Poux, P. Fayolle, J. Bertrand, D. Bridoux, J. Bousquet, Powder Technology (1991).

Appendix

The MATLAB code given below reconstructs a synthetic trajectory in 3D.

```
% test the 3D analytical reconstruction
clear
clc


% rng (4566809)
% assume the distance between two sensors is 0.1
sensortable = [0 0 0  1 0 0
               0 0 0  0 1 0
               0 0 0  0 0 1
              0.1 0 0 1 0 0
              0.1 0 0 0 1 0
              0.1 0 0 0 0 1];

for k = 1:100

  X = [rand(1,6)]*0.1;                          % generate random
particles
  X(2) = X(2)+0.05;
  X(4:6) = X(4:6)/norm(X(4:6))*0.1;             %normalize the moment
to 0.1
  T(k,:) = X;


  Z = Mag_dipole(X,sensortable);                 %generate the field
  [R,M,err] = MPT_recon(Z(1:3),Z(4:6),0.1);
  new_X(k,:) = R;
  new_M(k,:) = M;

  acc_err(k) = err;

% normalized position error
  error (k) = norm(X(1:3)-R)/0.1;

%normalized inner product, 1 means well aligned
  error_ang(k) = X(4:6)*M'/0.01;

end

% normalised error calculation
  posi_error = sum(error>0.1)/100;
  orientation_error = sum(error_ang<0.8)/100;

% error plots

figure, plot(error)
figure, plot(error_ang)

% plotting the reconstruction
```

```
t = 1:1:100;

figure

 plot(t,T(:,4),'-r.', 'MarkerSize', 10)
 hold on
 grid on
 plot(t,new_M(:,1)/0.1,'b-', 'LineWidth', 2)
 hold off
 xlabel('time')
 ylabel('Mx')

figure

 plot(t,T(:,5),'-r.', 'MarkerSize', 10)
 hold on
 grid on
 plot(t,new_M(:,2)/0.1,'b-', 'LineWidth', 2)
 hold off
 xlabel('time')
 ylabel('My')

figure

 plot(t,T(:,6),'-r.', 'MarkerSize', 10)
 hold on
 grid on
 plot(t,new_M(:,3)/0.1,'b-', 'LineWidth', 2)
 hold off
 xlabel('time')
 ylabel('Mz')

figure

 plot(t,T(:,1),'r.', 'MarkerSize', 10)
 hold on
 grid on
 plot(t,(new_X(:,1)/0.1),'b-', 'LineWidth', 2)
 hold off
 xlabel('time')
 ylabel('x')

figure

 plot(t,T(:,2),'r.', 'MarkerSize', 10)
 hold on
 grid on
 plot(t,(new_X(:,2)-0.05)/0.1,'b-', 'LineWidth', 2)
 hold off
 xlabel('time')
 ylabel('y')

figure

 plot(t,T(:,3),'r.', 'MarkerSize', 10)
 hold on
```

```
 grid on
 plot(t,(new_X(:,3)/0.1),'b-', 'LineWidth', 2)
 hold off
 xlabel('time')
 ylabel('z')


%%%%%%%%%%%%%%%%%%%%%%%%%%%%%%%%%%%%%%%%%%%%%%%%%%%%%%%%%%%%%%%%

% function to calculate the field

function z=Mag_dipole(S, sensortable)

[m,n]=size(sensortable);
z=zeros(m,1);


for i=1:m

    R=S(1:3)-sensortable(i,1:3);
    rr=norm(R);
    Moment=S(4:6);
    B=3*Moment*R'*R/rr^5-Moment/rr^3;

%by multiplication of this magnetic field with the orientation of
the sensor the signal strength can be estimated

    z(i)=B*sensortable(i, 4:6)';

end

z=z*1e-1;

%%%%%%%%%%%%%%%%%%%%%%%%%%%%%%%%%%%%%%%%%%%%%%%%%%%%%%%%%%%%%%%%


% This function reconstructs the 3D position and orientation of a
magnet
% The numerical method is based on Newton method

function [X,M,error,newbeta,newbetap1,newbetam1] =
MPT_recon(B1_raw,B2_raw,L,newbeta,newbetap1,newbetam1)

if nargin == 3

    beta = linspace(0,2*pi,360);
    all_recon = -ones(length(beta),7);

    for i = 1:length(beta)

        Rot = [1,0, 0; 0, cos(beta(i)),-sin(beta(i));0
sin(beta(i)),cos(beta(i))];
        B1=Rot*B1_raw;
        B2=Rot*B2_raw;
```

```
        if abs(B1(3))<1e-6
            B1(3)=1e-6;
        end
        if abs(B2(3))<1e-6
            B2(3)=1e-6;
        end

        T1=[B1(1);B1(2)]/B1(3);
        T2=[B2(1);B2(2)]/B2(3);
        D=T2(2)^2-T1(2)^2+T2(1)^2-T1(1)^2;
        E=(T1(1)*T2(2)-T2(1)*T1(2))/4;
        Cx=((T1(1)-T2(1))*D-(T1(2)-T2(2))*E)/((T1(1)-
T2(1))^2+(T1(2)-T2(2))^2);
        Cy=((T1(2)-T2(2))*D+(T1(1)-T2(1))*E)/((T1(1)-
T2(1))^2+(T1(2)-T2(2))^2);


S=((norm(T1))^2+(norm(T2))^2+(T1(1)+T2(1))*Cx+(T1(2)+T2(2))*Cy-...
            4*Cx^2-4*Cy^2)^0.5/2;

        if imag(S)~=0
            continue
        end

%         two possible solutions
        Mx=Cx-S*(T1(2)-T2(2))/norm(T1-T2);
        My=Cy+S*(T1(1)-T2(1))/norm(T1-T2);
        tan_1=(T1(2)-My)/(T1(1)-Mx);
        tan_2=(T2(2)-My)/(T2(1)-Mx);
        x=L*tan_2/(tan_2-tan_1);
        y=tan_1*x;
        mz1=-(norm([x,y]))^3*B1(3)*10;  %the unit of T
        mz1_= -(norm([x-L,y]))^3*B2(3)*10;

        Mx=Cx+S*(T1(2)-T2(2))/norm(T1-T2);
        My=Cy-S*(T1(1)-T2(1))/norm(T1-T2);
        tan_1=(T1(2)-My)/(T1(1)-Mx);
        tan_2=(T2(2)-My)/(T2(1)-Mx);
        x=L*tan_2/(tan_2-tan_1);
        y=tan_1*x;
        mz2=-(norm([x,y]))^3*B1(3)*10;
        mz2_= -(norm([x-L,y]))^3*B2(3)*10;

        if abs(mz1-mz1_)<abs(mz2-mz2_)
            mz=(mz1+mz1_)/2;
            Mx=Cx-S*(T1(2)-T2(2))/norm(T1-T2);
            My=Cy+S*(T1(1)-T2(1))/norm(T1-T2);
            tan_1=(T1(2)-My)/(T1(1)-Mx);
            tan_2=(T2(2)-My)/(T2(1)-Mx);
            x=L*tan_2/(tan_2-tan_1);
            y=tan_1*x;
        else
            mz=(mz2+mz2_)/2;
            Mx=Cx+S*(T1(2)-T2(2))/norm(T1-T2);
            My=Cy-S*(T1(1)-T2(1))/norm(T1-T2);
            tan_1=(T1(2)-My)/(T1(1)-Mx);
```

```
            tan_2=(T2(2)-My)/(T2(1)-Mx);
            x=L*tan_2/(tan_2-tan_1);
            y=tan_1*x;
        end

%       calculate all the values
        moment=[Mx*mz; My*mz; mz];

        Tmp_X = Rot'*[x,y,0]';
        Tmp_M = Rot'*moment;

%       The reconstructed error
        rr = norm(Tmp_X);
        B1_recon=(3*Tmp_X'*Tmp_M*Tmp_X/rr^5-Tmp_M/rr^3)*0.1;
%        the unit is micro T
        Tmp_R = [L,0,0]' - Tmp_X;
        rr = norm(Tmp_R);
        B2_recon=(3*Tmp_R'*Tmp_M*Tmp_R/rr^5-Tmp_M/rr^3)*0.1;

        all_recon(i,1:6)=[Tmp_X',Tmp_M'];
        all_recon(i,7) = norm(B1_recon-B1_raw)+norm(B2_recon-
B2_raw);

    end

%     remove the meaningless beta and find the best beta
      all_recon(all_recon(:,7)==-1,:)=[10];

    [error,index] = min(all_recon(:,7));

    if index ~= 1 && index ~=360
     newbeta= beta(index);
     newbetap1 = beta((index+1));
     newbetam1 = beta((index-1));
    elseif index == 1
     newbeta= beta(index);
     newbetap1 = beta((index+1));
     newbetam1 = beta(index);
    elseif index == 360
     newbeta= beta(index);
     newbetap1 = beta(index);
     newbetam1 = beta((index-1));
    end

    X = all_recon(index,1:3);
    M = all_recon(index,4:6);

%     recall the function to improve accuracy
test = 0;
while error > 1e-05 && test <= 500
      [X,M,error,newbeta,newbetap1,newbetam1] =
MPT_recon(B1_raw,B2_raw,L,newbeta,newbetap1,newbetam1);
      test = test +1;
end

elseif nargin > 3
```

```
    beta = linspace(newbetap1,newbetam1,100);
    all_recon = -ones(length(beta),7);

    for i = 1:length(beta)

        Rot = [1,0, 0; 0, cos(beta(i)),-sin(beta(i));0
sin(beta(i)),cos(beta(i))];
        B1=Rot*B1_raw;
        B2=Rot*B2_raw;

        if abs(B1(3))<1e-6
            B1(3)=1e-6;
        end
        if abs(B2(3))<1e-6
            B2(3)=1e-6;
        end
        T1=[B1(1);B1(2)]/B1(3);
        T2=[B2(1);B2(2)]/B2(3);
        D=T2(2)^2-T1(2)^2+T2(1)^2-T1(1)^2;
        E=(T1(1)*T2(2)-T2(1)*T1(2))/4;
        Cx=((T1(1)-T2(1))*D-(T1(2)-T2(2))*E)/((T1(1)-
T2(1))^2+(T1(2)-T2(2))^2);
        Cy=((T1(2)-T2(2))*D+(T1(1)-T2(1))*E)/((T1(1)-
T2(1))^2+(T1(2)-T2(2))^2);


S=((norm(T1))^2+(norm(T2))^2+(T1(1)+T2(1))*Cx+(T1(2)+T2(2))*Cy-...
            4*Cx^2-4*Cy^2)^0.5/2;
        if imag(S)~=0
            continue
        end

%       two possible solutions
        Mx=Cx-S*(T1(2)-T2(2))/norm(T1-T2);
        My=Cy+S*(T1(1)-T2(1))/norm(T1-T2);
        tan_1=(T1(2)-My)/(T1(1)-Mx);
        tan_2=(T2(2)-My)/(T2(1)-Mx);
        x=L*tan_2/(tan_2-tan_1);
        y=tan_1*x;
        mz1=-(norm([x,y]))^3*B1(3)*10;  %the unit of uT
        mz1_= -(norm([x-L,y]))^3*B2(3)*10;

        Mx=Cx+S*(T1(2)-T2(2))/norm(T1-T2);
        My=Cy-S*(T1(1)-T2(1))/norm(T1-T2);
        tan_1=(T1(2)-My)/(T1(1)-Mx);
        tan_2=(T2(2)-My)/(T2(1)-Mx);
        x=L*tan_2/(tan_2-tan_1);
        y=tan_1*x;
        mz2=-(norm([x,y]))^3*B1(3)*10;
        mz2_= -(norm([x-L,y]))^3*B2(3)*10;

        if abs(mz1-mz1_)<abs(mz2-mz2_)
            mz=(mz1+mz1_)/2;
            Mx=Cx-S*(T1(2)-T2(2))/norm(T1-T2);
            My=Cy+S*(T1(1)-T2(1))/norm(T1-T2);
```

```
            tan_1=(T1(2)-My)/(T1(1)-Mx);
            tan_2=(T2(2)-My)/(T2(1)-Mx);
            x=L*tan_2/(tan_2-tan_1);
            y=tan_1*x;
        else
            mz=(mz2+mz2_)/2;
            Mx=Cx+S*(T1(2)-T2(2))/norm(T1-T2);
            My=Cy-S*(T1(1)-T2(1))/norm(T1-T2);
            tan_1=(T1(2)-My)/(T1(1)-Mx);
            tan_2=(T2(2)-My)/(T2(1)-Mx);
            x=L*tan_2/(tan_2-tan_1);
            y=tan_1*x;
        end


%       calculate all the values
        moment=[Mx*mz; My*mz; mz];

        Tmp_X = Rot'*[x,y,0]';
        Tmp_M = Rot'*moment;

%       The reconstructed error
        rr = norm(Tmp_X);
        B1_recon=(3*Tmp_X'*Tmp_M*Tmp_X/rr^5-Tmp_M/rr^3)*0.1;
%        the unit is micro T
        Tmp_R = [L,0,0]' - Tmp_X;
        rr = norm(Tmp_R);
        B2_recon=(3*Tmp_R'*Tmp_M*Tmp_R/rr^5-Tmp_M/rr^3)*0.1;

        all_recon(i,1:6)=[Tmp_X',Tmp_M'];
        all_recon(i,7) = norm(B1_recon-B1_raw)+norm(B2_recon-
B2_raw);
    end

%     remove the meaningless beta and find the best beta
      all_recon(all_recon(:,7)==-1,:)=[10];

    [error,index] = min(all_recon(:,7));

    if index ~= 1 && index ~=100
     newbeta= beta(index);
     newbetap1 = beta((index+1));
     newbetam1 = beta((index-1));
    elseif index == 1
     newbeta= beta(index);
     newbetap1 = beta((index+1));
     newbetam1 = beta(index);
    elseif index == 360
     newbeta= beta(index);
     newbetap1 = beta(index);
     newbetam1 = beta((index-1));
    end

    X = all_recon(index,1:3);
    M = all_recon(index,4:6);
```

```
end

end

%%%%%%%%%%%%%%%%%%%%%%%%%%%%%%%%%%%%%%%%%%%%
```